Development of LIF based tomography technique for studying turbulent shear flows

A Thesis
Submitted for the Degree of
MASTER OF SCIENCE (ENGINEERING)

by

KANWAR NAIN SINGH

ENGINEERING MECHANICS UNIT
JAWAHARLAL NEHRU CENTRE FOR ADVANCED SCIENTIFIC RESEARCH
(A Deemed University)
Bangalore – 560 064

OCTOBER 2014

To my Parents

DECLARATION

I hereby declare that the matter embodied in the thesis entitled **"Development of LIF based tomography technique for studying turbulent shear flows"** is the result of investigations carried out by me at the Engineering Mechanics Unit, Jawaharlal Nehru Centre for Advanced Scientific Research, Bangalore, India under the supervision of **Prof. K. R. Sreenivas** and that it has not been submitted elsewhere for the award of any degree or diploma.

In keeping with the general practice in reporting scientific observations, due acknowledgment has been made whenever the work described is based on the findings of other investigators.

_____

Kanwar Nain Singh

CERTIFICATE

I hereby certify that the matter embodied in this thesis entitled **"Development of LIF based tomography technique for studying turbulent shear flows"** has been carried out by **Mr. Kanwar Nain Singh** at the Engineering Mechanics Unit, Jawaharlal Nehru Centre for Advanced Scientific Research, Bangalore, India under my supervision and that it has not been submitted elsewhere for the award of any degree or diploma.

Prof. K. R. Sreenivas
(Research Supervisor)

ACKNOWLEDGEMENT

I owe my gratitude to Prof. K. R. Sreenivas for his guidance and constant encouragement. His expertise in experiments and deep physical insights into the problem helped me a lot in carrying forward my work. I especially value the freedom that he gave, initial while choosing the problem and later for carrying out my work.

I am also grateful to Prof. Ganesh Subramanian, Prof. Mehboob Alam, Prof. Rama Govindrajan, Dr. Santosh Ansumali and Dr. Arindam Chakraborty (CAOS, IISc) for their invaluable coursework which benefited me a lot.

I would like to thank all my lab-mates (Dhiraj, Shashank, Siddharth, Vybhav, Rafi, Nakul and a pseudo lab-mate, Sunil) for helping me during experiments and for all the fun time we had in the lab. I would also like to thank all my friends in JNC for making my stay a memorable one. Thanks to Prasanth, Deepak, Milind, Vicky, Rajesh, Sankalp, Ponnu, Deepthi, Chakri, Navaneeth and Saikishan for all the interesting discussions, to Siddharth, Milind for the bike trips, to Rafi, Achal, Ronak and Milind for late night Bournvita and discussions, and to Meha and Priyanka for the awesome food they cooked. Special thanks to all the football buddies who really helped a lot in making my stay in JNC a fun time.

Above all, I would like to thank my parents for the unconditional love and support.

ABSTRACT

Clouds are one of the major sources of uncertainty in climate prediction (IPCC Fourth Assessment Report: Climate Change 2007). They play a significant role in transporting heat across the whole extent of the troposphere. Cloud formation and its development is a complex phenomenon, because of which until recently no effective laboratory studies were done on clouds, because there was no technique or apparatus that could handle those complexities (Stratmann *et al.*, 2009). Narasimha *et al.* (2011) were able to successfully reproduce a variety of cloud forms occurring in nature. They presented "the transient plume subjected to off-source diabatic heating" as an appropriate model for simulating cloud flows.

Taking lead from there, we planned to study the entrainment characteristics of orographic clouds in laboratory. We modeled orographic clouds as diabatic, planar turbulent, wall-jets. Validation of such a model would be easier in the field compared to free standing clouds, as instruments can be placed along the terrain to measure the actual flow conditions. Also, the two dimensionality of the planar wall jet makes it closer analogue to an orographic cloud as they rise as a layer hugging along the mountain slope. We subject this wall jet to volumetric heating to understand the impact of phase change on its turbulence structures.

We designed and fabricated an apparatus which is capable of producing a continuous turbulent and two dimensional wall jet. A provision was made such that the complete wall jet apparatus could be made inclined to a desired angle to the vertical, to mimic the mountain slope. Initial flow visualization showed that the apparatus was capable of producing a two-dimensional wall jet at various angles. A set of heating grids were designed and fixed parallel to the wall in order to volumetrically heat the flow to mimic the latent heat released due to condensation in real clouds, a technique first described by Bhat et. at. (1989).

Planar laser induced fluorescence (PLIF) experiments were also performed with and without heating. It was found that that the scalar width of a wall jet decreases drastically with the addition of heat which is consistent with orographic clouds rising like a thin sheet along the mountain slope.

We also developed a new technique for three dimensional scanning laser induced fluorescence. All the materials used for the development were conveniently available and were relatively cheaper than those used in all previously developed techniques. This technique could be used to study the time evolution of scalar field in turbulent flows. Basically, the laser sheet was made to scan the flow and images at various sections were captured using a high speed camera. After rigorous image processing, the data was used to reconstruct the three dimensional concentration fields. In order to check for the robustness of the technique, it was used for an axisymmetric round jet. The extracted data was well in agreement with the previous literature.

TABLE OF CONTENTS

LIST OF FIGURES

CHAPTER 1

INTRODUCTION

1.1. Introduction

Man has been always fascinated by the beauty of clouds so much so that poets, artists and photographers portray the beauty and majesty of clouds in their creative works. In this modern era, clouds caught the interest of meteorologists because of their significant impact on climate. Clouds are one of the major sources of uncertainty in climate prediction (IPCC Fourth Assessment Report: Climate Change 2007), which was listed in "the most urgent scientific problem requiring attention" by the Intergovernmental panel on climate change (Second Assessment Report (SAR) - IPCC 1995).

Figure 1.1: Image of cumulus clouds taken from an airplane.

Understanding cloud physics is important as clouds have a very significant effect on earth's atmosphere. Global warming is one of the biggest problems the planet earth is facing right now. Ramaswamy *et al.* (2001) gave an estimate that a 5% increase in short wave cloud would result in a forcing that would be adequate enough to clear all the effects of the greenhouse gases emitted between 1750 and 2000. Svensmark (1997) gave an alternate theory, describing the effects of cosmic rays on cloud formation as an indirect cause of global warming. He claims that human influence and the effect of greenhouse gases had been exaggerated. Later in 2008, this new theory was criticized by Lockwood and Fröhlich (2008). They concluded that the correlation between the observed increase in mean global temperature and solar variability was so poor that no causal mechanism could be ascribed to it, although they accepted that there was "considerable evidence" for solar influence on Earth's pre-industrial climate and to some degree also for climate changes in the first half of the 20^{th} century. Nevertheless, in any case it was implied that clouds do play an important role in global warming.

Some salient features of clouds in general and cumulus clouds in particular were described by Houze Jr (1994) and Narasimha (2012). These features can be summarized as follows: clouds are "a visible aggregate of minute particles of water or ice or both in the free air". Most commonly seen cloud called cumulus cloud (derived from Latin word *Cumulo* which means "heap" or "pile") having distinctive shapes, is certainly the most important cloud type because of its scientific importance, especially in the tropics. These clouds can sometimes grow all the way till tropopause and are thus known to transport heat over the whole vertical extent of the atmosphere. Clouds exhibit a wide variety of shapes and sizes, and each one has some specific significance in global atmospheric circulation. Luke Howard, a British chemist in 1802 devised a nomenclature and divided all clouds into finite number of characteristic forms. Cumulus clouds were defined as "detached clouds, generally dense and with sharp outlines, developing

vertically in the form of rising mounds, domes or towers, of which the bulging upper part often resembles a cauliflower". Usually the lifespan of these clouds is in the order of few minutes to few hours while the eddy turnover time for the same ranges from tens of seconds to few minutes, which means that typical cumulus cloud is usually transient in nature (Chandrasekhar, 2010). Charney and Shukla (1981) suggested that climate changes should be inherently more predictable in the tropics than in the higher latitudes. But the inadequacy of the present modelling techniques to handle moist convection leaves this potential predictability unexploited till date.

Cumulus clouds are formed when a moist air mass is forced to rise because of orographic lift or when warm and moist air mass rises upwards from a hot patch in the form of plume. The temperature of the rising air mass reduces, due to adiabatic expansion. After rising to some height, the relative humidity becomes 100% and water vapour present in the parcel starts to condense. This vertical position is known as lifted condensation level (LCL) or cloud base. As vapour condenses, the latent heat is released back into the parcel. Thus as the result of phase change, reduction of temperature due to adiabatic expansion is subdued for a moist parcel beyond cloud base. This process in turn, leads to local enhancement of buoyancy and the cloud rises even higher. This local enhancement of buoyancy plays a significant role in determining the rate of entrainment, and shape and size of the cloud. Therefore, cloud formation and its development is a complex phenomenon, which includes 1) mass transport by cumulus convection, 2) generation of liquid and/or ice phases of water, 3) interactions with the sub-cloud-layer, 4) interactions with radiation, and 5) mechanical interactions with mean flow (Arakawa, 2004).

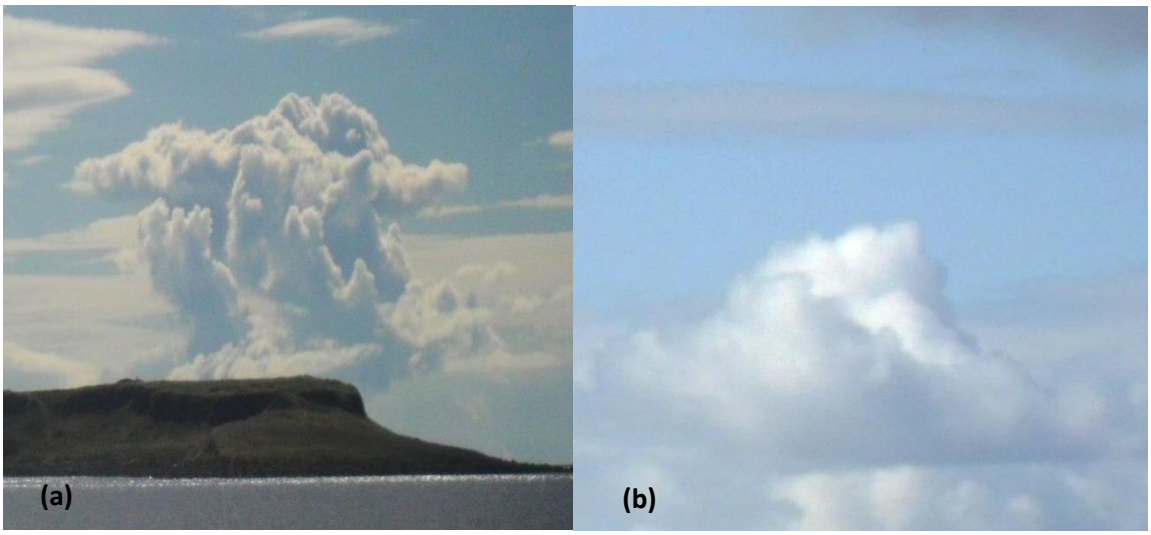

Figure 1.2: Two typical cumulus cloud types: (a) Tower-like (b) Tomb-like.

Owing to these complexities, until recently no effective laboratory studies were done on clouds, because there was no technique or apparatus that could handle those complexities (Stratmann *et al.*, 2009). Hence, the research on clouds was exclusively dependent on field studies (using radars and/or aircrafts). But the results were not robust enough as occurrence of clouds is very intermittent in space and time (Narasimha, 2012).

A major area of interest for scientists in understanding cloud dynamics is the process of entrainment (mixing of dry ambient air with the cloud parcel); as this process significantly affects the characteristic features of clouds such as the shape of the cloud, rate of ascent and its dilution. So understanding entrainment in clouds could help in better parameterization and thus help in producing a better weather forecast.

1.2. Early Models

Reuter (1986) presented a comprehensive review on entrainment models. Over the years, several entrainment models have come up. First proposal came up in 1947 by Stommel (1947) which stated that dry air gets entrained laterally from its surroundings. Measurements made by Malkus (1954) also supported this argument. Warner (1955) had an alternate view and said that the entrainment from the cloud top was the important factor and not lateral mixing. Ludlam and Scorer (1957) presented an idea of a thermal or a point buoyancy source as an appropriate model for clouds. Later Turner (1963, 1983) presented various models ranging from thermals, a solution from Hill's spherical vortex, lateral mixing in plumes to a starting plume model (Figure 1.3). The measurements made by Sloss (1967) and observations by Paluch (1979) completely discarded the idea of lateral mixing. According to Paluch (1979), the observed cloud heights could only be achieved only if there was a minimal lateral mixing with the ambient air. He suggested that the penetrative downdraft was the mechanism for dilution. Even Squires and Turner (1962) observed the same. The lateral mixing models failed to make realistic estimates of either liquid-water concentrations or height of the penetration for clouds. Moreover, the observed Riehl-Malkus protected cores also could not be explained by any of the above models.

These observations made it clear that Taylor's hypothesis (Taylor, 1946), which states that mean inwards entraining fluid velocity is proportional to characteristic local velocity and which very well predicted the entrainment in numerous practical flows like classical jets and plumes (Morton *et al.*, 1956), could not be extended to cloud flows, because of the transient nature of such flows. Simpson (1983) summarized early models for entrainment and mixing phenomenon in clouds. Emanuel (1994) discarded these cloud entrainment models as those were not in agreement with the observations. Blyth (1993) reasoned that

the entrainment "anomalies" were because of the assumption of self-similarity, which is not valid for clouds.

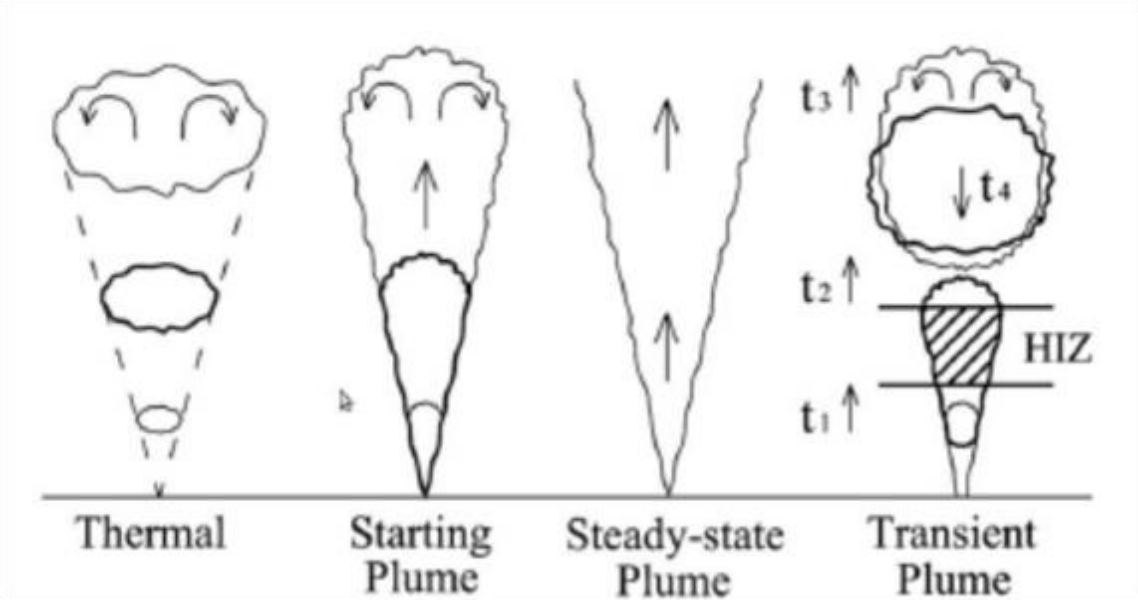

Figure 1.3: Schematic of different cumulus cloud evolution models. (Narasimha *et al.*, 2011).

Some other flow models such as episodic vertical mixing (Squires, 1958 and Telford, 1975) and shedding thermals model (Blyth, 1993) had been able to explain the characteristic entrainment features, at least near the cloud top. Also some recent studies suggested that lateral mixing was highest near the cloud base and drops at higher altitudes (Romps *et al.*, 2010 and Heus *et al.*, 2008). But so far no entrainment model has been able to explain this observation.

1.3. Cloud flow Models

Turner (1973) suggested that cloud formation and development could be put into a class of turbulent shear flows, more specifically to a class of thermals and plumes. Turner (1969) and List (1982) had given comprehensive detailed review of plumes. Latent heat released during condensation of water vapour in a cloud adds extra buoyancy to fluid, thereby making it different from classical plumes. According to Turner (1986), the continuous engulfment of dry ambient fluid into the core fluid was because of large eddies followed by some small scale mixing across the core with constant entrainment coefficient.

As discussed earlier, the entrainment hypothesis by Taylor (1946) which was being used to understand flow development in various geophysical flows, failed to make realistic estimates for cloud flows. Until recently, none of the flow models were able to mimic macro dynamics of cumulus clouds. Bhat *et al.* (1989) developed a technique to locally enhance buoyancy by volumetrically heating the flow (plume). A detailed analysis of this setup was presented by Bhat and Narasimha (1996). They reported that entrainment coefficient in a volumetrically heated jet was significantly different from that in a self-similar jet. Venkatakrishnan (1998) also did a quantitative study using similar setup. Their Planar Laser Induced Fluorescence (PLIF) images showed drastic reduction in heated plume width compared to classical plumes. They also showed that dilution in core fluid was negligible which was consistent with protected cores observed in cumulus clouds by Riehl and Malkus (1958). They suggested that it was the disruption of coherent eddy structures which leads to reduction in entrainment. Similar studies reported by Venkatakrishnan *et al.* (2003) and Agarwal and Prasad (2004) observed similar phenomenon. A comprehensive review of these works was presented by Diwan *et al.* (2011).

Narasimha *et al.* (2011) re-plotted the variation in entrainment coefficient along the streamwise direction above the cloud base for all previous laboratory studies (figure 1.4). The data presented a trend very different from steady state plumes or any other entrainment models. There was mild increase in entrainment during the initial part of heat injection zone and it subsequently falls below self-similar value. These results were broadly consistent with real cloud measurements (Narasimha, 2012). But the entrainment coefficient variation presented by Agarwal and Prasad (2004) was very different from that observed in all other experiments. Narasimha and Bhat (2008) attributed this disagreement to high electrical conductivity of jet fluid which resulted in much higher heat addition than observed in real clouds.

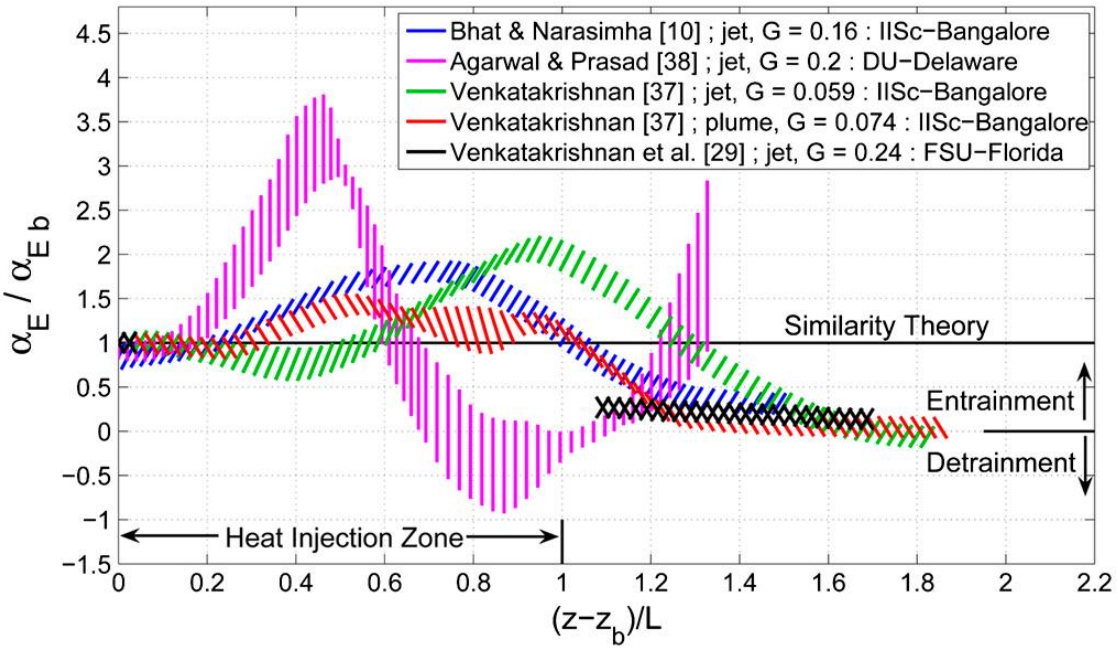

Figure 1.4: Entrainment coefficient variation from all the experiments on cloud-like flows. (Narasimha *et al.*, 2011)

In recent experiments, Narasimha *et al.* (2011) were able to produce variety of naturally occurring cloud types and were also able to track their history. Based on these experiments, they suggested that off source volumetric heating,

dynamically scaled to mimic latent heat release due to condensation in a cloud, plays an important role in determining certain features of the cloud. They presented "the transient plume subjected to off-source diabatic heating" as the appropriate model for simulating cloud flows. Some of the important cloud types simulated in this experiment are shown in figure 1.5 in comparison with real clouds (left) (Narasimha *et al.*, 2011).

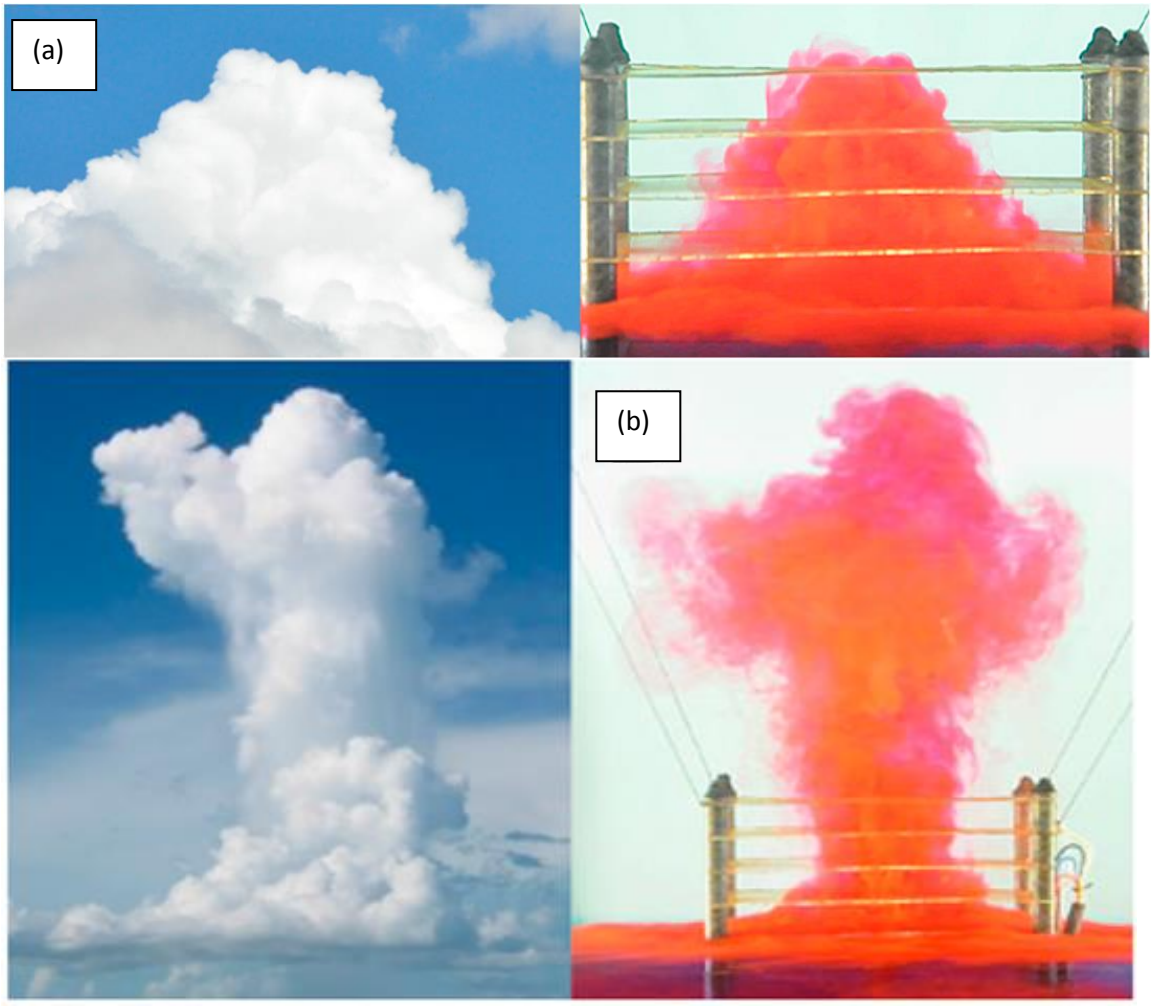

Figure 1.5: Two important types of clouds produced in lab. (Narasimha *et al.*, 2011)

Some numerical simulations have also been reported on cloud flows. Basu and Narasimha (1999) simulated a temporally evolving jet with volumetric heat addition. Recently Prasanth (2014) reported a direct numerical simulation of a transient diabetic plume. Their observations were consistent with experiments. They suggested that the distortion of coherent eddy structures results in dramatic increase in vorticity post heat injection zone, and aids in altering the entraining flow field (Sreenivas, 2004).

A theoretical model was presented by Sreenivas and Prasad (2000) have explained the mechanism for entrainment in jets and plumes and for flows with volumetric heat addition (cloud flows). Their entrainment mechanism was based on vortex dynamics in a flow with axial stretching. They suggested that entrainment does not depend much on local vorticity, but on axial bouncy gradient. They concluded that it was the opposing baroclinic torque (arising because of axial temperature difference due to volumetric heating) which causes the reduction in entrainment. Sreenivas (2004), by means of numerical simulation, showed that the axial acceleration suppresses the formation of large scale structures and in turn, reduces the entrainment which was consistent with the above mentioned model. In contrast, Basu and Narasimha (1999) model primarily depends on radial temperature gradients. The believed that the baroclinic torque resulting from radial temperature differences forces engulfment tongues to fold and reduces entrainment because of enhanced shear.

In the present study, we present a laboratory flow model for orographic cloud like flow. A quantitative study on effect of off source heating on entrainment is reported here. We also report a new technique for three dimensional scanning planar laser induced fluorescence and validation of the technique for axisymmetric round jet which will help in quantifying entrainment in transient non-self similar flows.

CHAPTER 2

OROGRAPHIC CLOUDS

2.1. Introduction

Orographic lift is defined as the phenomenon in which air is forced to rise to higher altitudes because of surface topology or mountains. Orographic clouds are formed when moist air-parcel is forced to rise above lifted condensation level along a mountain slope. As the vapour present in the air-parcel starts to condense, the latent heat of condensation is released into the air-parcel which leads to enhancement of buoyancy locally. The enhanced buoyancy, beyond the condensation level, experienced by the moist air-parcel is believed to be responsible for giving a unique characteristic feature to a cloud. In the present study, we plan to study the effect of latent heat release on the cloud flow properties.

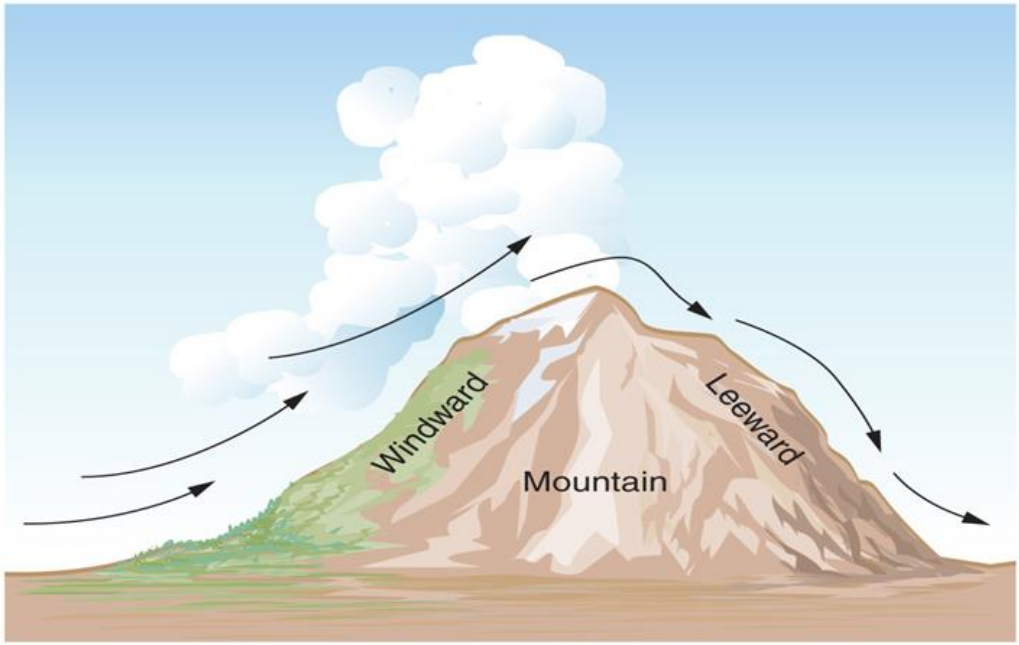

Figure 2.1: Illustration of orographic lift (Image credits: NOAA/NWS).

2.2. Orographic Flow Regimes

When the wind blowing near the surface encounters a mountain, the flow can either detour around the mountain or rise over it. This flow response largely depends upon the non-dimensional parameter, Froude number (Fr):

$$Fr = \frac{U}{NH}$$

where U is characteristic wind-velocity scale, H is mountain height, and N is the Brunt-Väisälä frequency, which is given by:

$$N^2 \approx \frac{g}{\rho_0}\frac{d\bar{\rho}(z)}{dz}$$

where $\bar{\rho}(z)$ is the vertical density profile in the atmosphere and ρ_0 is the density of air at the surface. Now when $N^2 > 0$, the atmosphere is statically stable; when $N^2 < 0$, the atmosphere is statically unstable; and when $N^2 = 0$, the atmosphere is statically neutral.

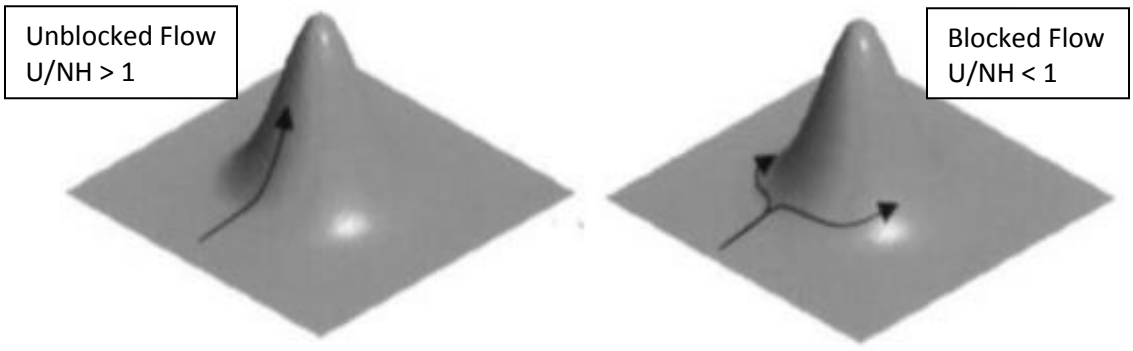

Figure 2.2: Schematic showing effect of Froude number on impinging flow. (Image taken from NCAS Atmospheric Measurement Summer School Brochure)

In fluid mechanics, Froude number is the ratio between inertial and gravitational forces. Basically, Froude number, in the context of present study, represents the ratio of the kinetic energy of the impinging wind to the potential energy gained by the air parcel after its ascend over the mountain. It is known that density decrease with height in the troposphere. At a given location, atmosphere will have an environmental lapse rate. If the moist air-parcel subjected to orographic lift, experiences a cooling more than the environmental lapse rate, then the air parcel will have a tendency to sink down to its original position. So when an air parcel is forced to ascend a mountain and if it becomes cooler and denser relative to its surroundings then it will have 'negative buoyancy'. Thus, the wind can flow over a hillock only if its kinetic energy could overcome this negative buoyancy, otherwise wind will flow around the hillock.

1. Blocked flow: When the flow is weak and is unable to overcome the retarding effects of negative buoyancy (Fr < 1), it detours around the mountain and this is known as blocked flow (Baines, 1987) (figure 2.2).
2. Unblocked flow: When Fr > 1, the flow possesses enough momentum to overcome the negative buoyancy which allows it to complete its ascent over the mountain. Now, the flow may either accelerate or decelerate while ascending along the mountain depending on the width of the mountain (Corby, 1954) (figure 2.2).

$$Fr_L = \frac{U}{NL}$$

where Fr_L is the Froude number based on width L of the mountain.

When impinging winds are strong, with weak atmospheric stability and flow is over a narrow mountain, the flow passes over the mountain too rapidly to be effected by the negative buoyant forces. Here, in this case, the flow accelerates because of Bernoulli's effect. This response is referred to as 'evanescent' as the

disturbance due to mountain fades away rapidly after the ridge. In contrast, when the flow is weak with considerably strong stability and flowing over a wide mountain, the flow spends enough time over the mountain slope to feel the lifting effect due to mountain. Negative buoyancy created in a stable atmosphere decelerates the ascending flow over the upwind side of the mountain. The mountain-waves created in this case are not only confined to area above the mountain, but can propagate both upwind and downwind sides of the mountain into the atmosphere.

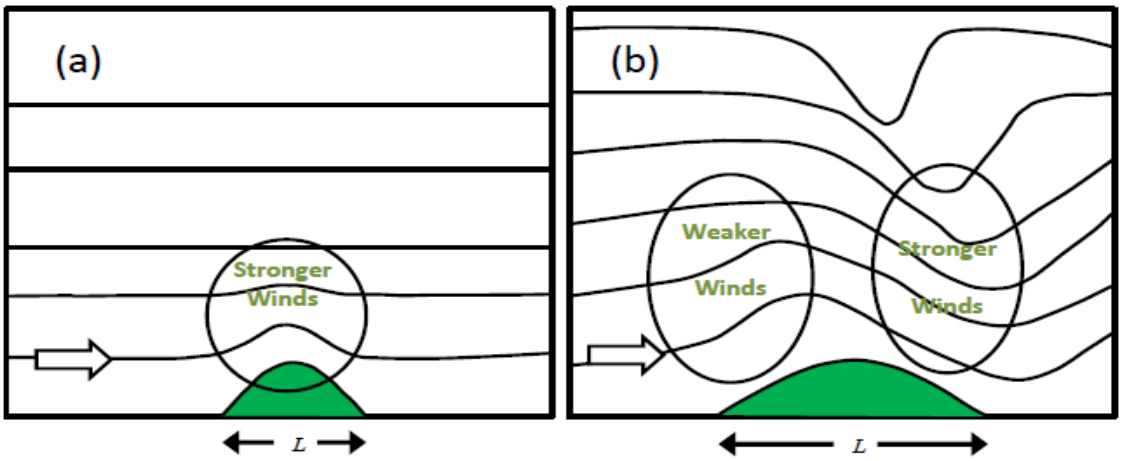

Figure 2.3: Comparison of vertical structures of (a) Evanescent flow and (b) Mountain (Lee) waves flow.

Figure 2.4: Image showing orographic cloud formation along a slope. (Collection of Dr. Igor Smolyar, NOAA Central library)

2.3. Motivation

Understanding the effects of orography is important as it has a strong effect on the monsoons, particularly for a country like India where monsoons are known to impact the country's economy significantly. Hahn and Manabe (1975) revealed that the presence of mountains is instrumental in maintaining the south Asian low pressure system. Observations and modeling results by Boos and Kuang (2010) suggested that the Himalayan Mountains insulate the warm, moist air over the continental India from the cold and dry air from extratropics. Ma *et al.* (2014) confirmed this idea that topography creates a strong monsoon by insulating the thermal maximum from dry extratropical air. So orography certainly has huge impact on Indian weather circulation. More importantly, Chakraborty *et al.* (2002)

had given an estimate that seasonal mean precipitation would reduce by 25% if orography was removed all around the world.

From the above discussion, it is clear that understanding the effect of orography will certainly improve the weather forecast system. Sawyer (1956) explains the physical and dynamical problems involved in study of orography induced rain. According to him, the inter relation between rainfall, height, aspect, wind direction, etc. is so complicated that to estimate the orographic rain, one needs to understand the physical mechanism behind orographic rain. Because of these complications, it was impossible to mimic the orographic effect as a whole in a laboratory experiment. But understanding and representing the effects of orography in numerical weather prediction models was of crucial importance for weather forecasting and climate prediction. Since the phenomena usually occur on scales which cannot explicitly be resolved by numerical integration of the basic equations (because of huge computational cost involved), such effects needed to be parameterized. Wang *et al.* (2004) gave a review on climate modelling. They also put forward the challenges involved in climate modelling because of orography. Scientists had been constantly working on to improve the parameterization schemes to have more accurate forecast. Dash and Mohandas (2005) did a comparative study of various orographic representations which were used for simulating Indian monsoon. A comprehensive review of studies related to flow over a hill was given by Belcher and Hunt (1998). According to them, current models do not represent several mechanisms, particularly those associated with distortion of vorticity and the structure of turbulence.

As discussed earlier orographic-cloud physics involves many complex issues. In the present study, our objective is to understand the role of buoyancy enhancement due to phase change on vorticity and turbulence structures in orographic clouds. Governing parameters could be formulated which in turn, could

be incorporated in the weather forecasting models to improve their accuracy. This forms the main motivation behind the present study.

2.4. Orographic Cloud Flow Model

In the present set of experiments, we plan to look into the turbulence structure of clouds rising along the mountain slope. Particularly, we are going to study the flow regime in which for Fr >> 1 and corresponds to a scenario in which the moist air impinges on to the mountain and then rises along the slope of the mountain. This orographic lift forces the parcel to rise above the lifted condensation level. The moisture in the air then starts to condense and the latent heat of condensation is released into the cloud air-mass. A set of studies (Bhat *et al.* (1989), Bhat & Narasimha (1996) and Narasimha *et al.* (2011)) had shown that the latent heat released in the phase change processes in a cloud has a significant impact on its entrainment and hence, the shape. These studies suggested that the heat addition probably plays an important role in describing the cloud flow structure in terms of vorticity and turbulence structure. They describe cumulus clouds as a 'transient diabatic plume'. Taking lead from here, we plan to apply the same mechanism to model orographic clouds. In orographic clouds, in addition to buoyancy enhancement due to phase change, they also have interaction with the mountain slope, which leads to continuous generation of vorticity. We believe, this is the first ever laboratory model to understand the dynamics of orographic clouds.

In this study, we model orographic clouds as diabatic, planar turbulent wall jets. The two dimensionality of the planar wall jet makes it closer analogue to an orographic cloud as they rise as a layer hugging along the mountain slope. We subject this wall jet to volumetric heating to understand the impact of phase change on its turbulence structures. Also, validation of such a model would be

easier in the field compared to free standing clouds, as instruments can be placed along the terrain to measure the actual flow conditions.

2.5. Wall Jets

Wall jet is defined as "a shear flow directed along a wall where, by virtue of the initially supplied momentum, at any situation, the streamwise velocity over some region within the shear flow exceeds that in the external stream" (Launder and Rodi, 1981). Wall jets have many engineering applications, most common would be car windshield defroster and on a large scale, airflow hugging the roof of Kansai International Airport, Japan, for HVAC application. The turbulent wall jet is of great interest for the researchers because of its two layer character. The wall layer resembles turbulent boundary layer and the outer layer is similar to a jet.

The ideal plane wall jet is the one being injected out from a slot of infinite aspect-ratio and has no restrictions in streamwise and transverse direction (George *et al.*, 2000). Typical wall jet velocity profile is shown in figure 2.5. The velocity is zero at the wall because of no slip condition, and is zero, as well, at some transverse distance away from the wall where wall jet meets the ambient fluid.

In a wall jet, there is momentum loss near the wall due to skin friction. As the wall jet flows downstream, it spreads in the direction normal to the wall. This is because of growth of the boundary layer near the wall and the engulfment of the ambient fluid from the outer region, which is known as entrainment (Rajaratnam, 1976). The jet half width $y_{1/2}$, which is the normal distance from the wall in the outer region where the velocity reduces to half of the maximum velocity, the growth of this length scale is used to quantify the rate of spread. The slope,

$dy_{1/2}/dx$ of a linear regression applied to the fully developed region indicates the spread of the wall jet (Launder and Rodi, 1981).

$$y_{1/2} = A(x - x_0)$$

where x_0 is the virtual origin and $A = dy_{1/2}/dx$, is a constant characteristic of the flow.

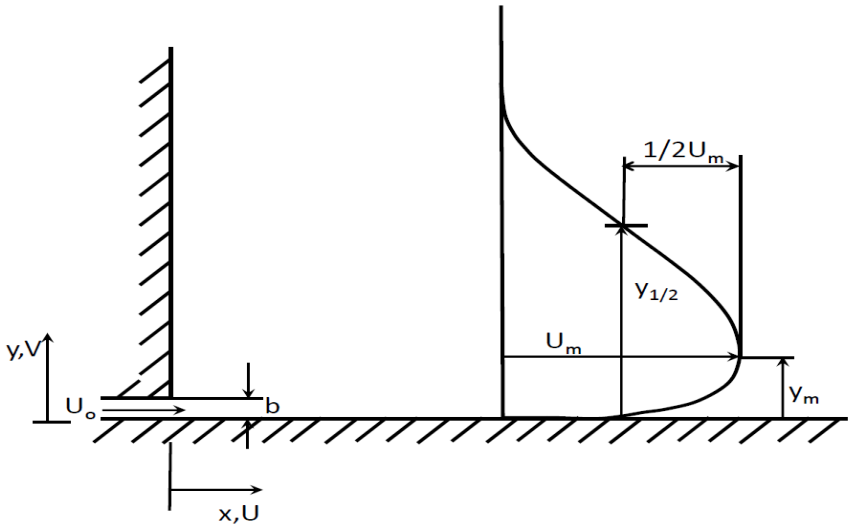

Figure 2.5: Velocity profile of a plane wall jet.

The loss of momentum at the wall and the momentum redistribution with the entrained fluid causes the maximum velocity U_m to decrease in the streamwise direction.

$$\frac{U_m}{U_o} = B\left(\frac{y_{1/2}}{b}\right)^n$$

where U_o is the nozzle exit velocity, b is the slot width and B is another constant (George *et al.*, 2000) characteristic of the flow.

2.5.1. Previous Studies on Wall Jets

The first comprehensive review of wall jet literature was presented by Launder and Rodi (1981). They assessed the quality of turbulent wall jet studies and discarded many studies which were not consistent or the results of which were not credible. For studies on planar wall jet, their principal test was the flow satisfying the two dimensional momentum integral equation. Based on the previous experimental studies, they determined a range for the slope of jet half-width, which is $dy_{1/2}/dx = 0.073 \pm 0.002$. Schneider and Goldstein (1994) did single component laser Doppler Velocimetry (LDV) measurements for turbulent plane wall jet in still air. They found that the LDV measurements shows significantly higher Reynolds shear stress in the outer region compared to the hot wire measurements. The most comprehensive experimental study of plane turbulent wall jet was done by Eriksson *et al.* (1998). They used a two component LDV system for highly resolved spatial measurements, especially in the near wall region which enabled them to determine wall shear stress and hence use the friction velocity, u^* as an inner velocity scale. They compared their data with previous studies and found that there were large differences between their LDV and previous hot wire turbulence data in the outer region. They attributed these differences to the limitation of the hot wires to measure the reverse flow. They determined the value of spread rate, $dy_{1/2}/dx$ as 0.078 and the decay rate, $d(\log(u_m))/d(\log(y_{1/2}))$ as -0.57 in the region along the flow from 40d to 150d, which they found to be self-similar.

George *et al.* (2000) gave a new similarity theory for plane wall jet in quiescent surroundings. They used asymptotic invariance principle (AIP) to find similarity solution in the limit of infinite Reynolds number. They showed that u^* and ϑ/u^* were the appropriate velocity and length scales in the inner region while u_m and $y_{1/2}$ were the appropriate ones for outer region. They also found that u_m

change follows power law in the form of $u_m = B(y_{1/2})^n$, where n needed to be less than -0.5 in order for similarity to be achieved. After applying the power law relation, they found the best fit value for n was -0.528. This theory was found to be in agreement with previous experimental results, particularly those of Eriksson *et al.* (1998).

Deojan and Laschziner (2004) presented a direct comparison to the experimental results of Eriksson *et al.* (1998) in a numerical study using large eddy simulation (LES) method. Their results appeared to be consistent with the experiments. They also provided the budgets for Reynolds stresses and turbulence energy, which allowed them to understand the interaction between the outer and inner layer.

Blarenblatt *et al.* (2005) used the experimental data of Karlsson *et al.* (1992) and hypothesized that turbulent wall jets consist of two layers: a free shear layer and a wall bounded layer, separated by a mixing layer where velocity is close to the maximum. They also demonstrated that there is incomplete similarity in the wall and free shear layer of wall jet as the scaling laws in these layers were substantially different. This made them to conclude that width of the slot has a strong influence on the development of a wall jet. The property on incomplete similarity was also confirmed by plotting $\ln(u_m/u_0)$ as a function of $\ln(x/b)$. It was found that the slope of linear fit to the data was -0.6, whereas the value for complete similarity as proposed by George *et al.* (2000) was -0.5.

2.6. Experimental Apparatus and Instrumentation

An experimental apparatus was designed and fabricated to produce a wall jet along with the provision to simulate heat release due to phase change. It consisted of a glass walled tank, a settling chamber, an acrylic wall, a constant head tank, a flow conditioner with a nozzle, a heating grid and a piping system capable of transferring water from the constant head tank to the settling chamber.

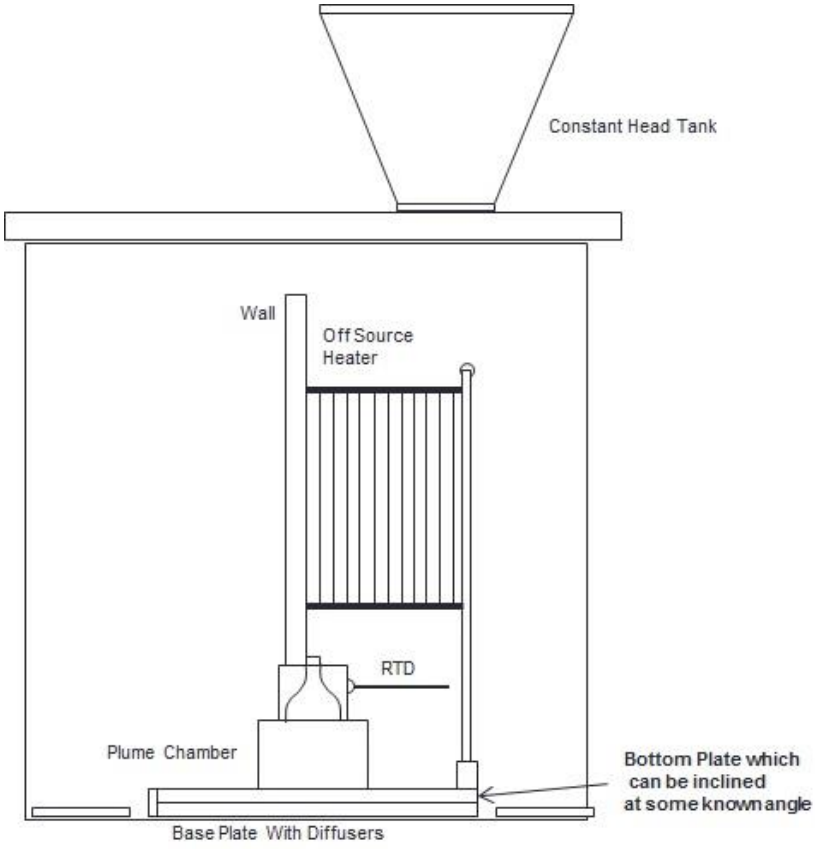

Figure 2.6: Schematic of wall jet apparatus.

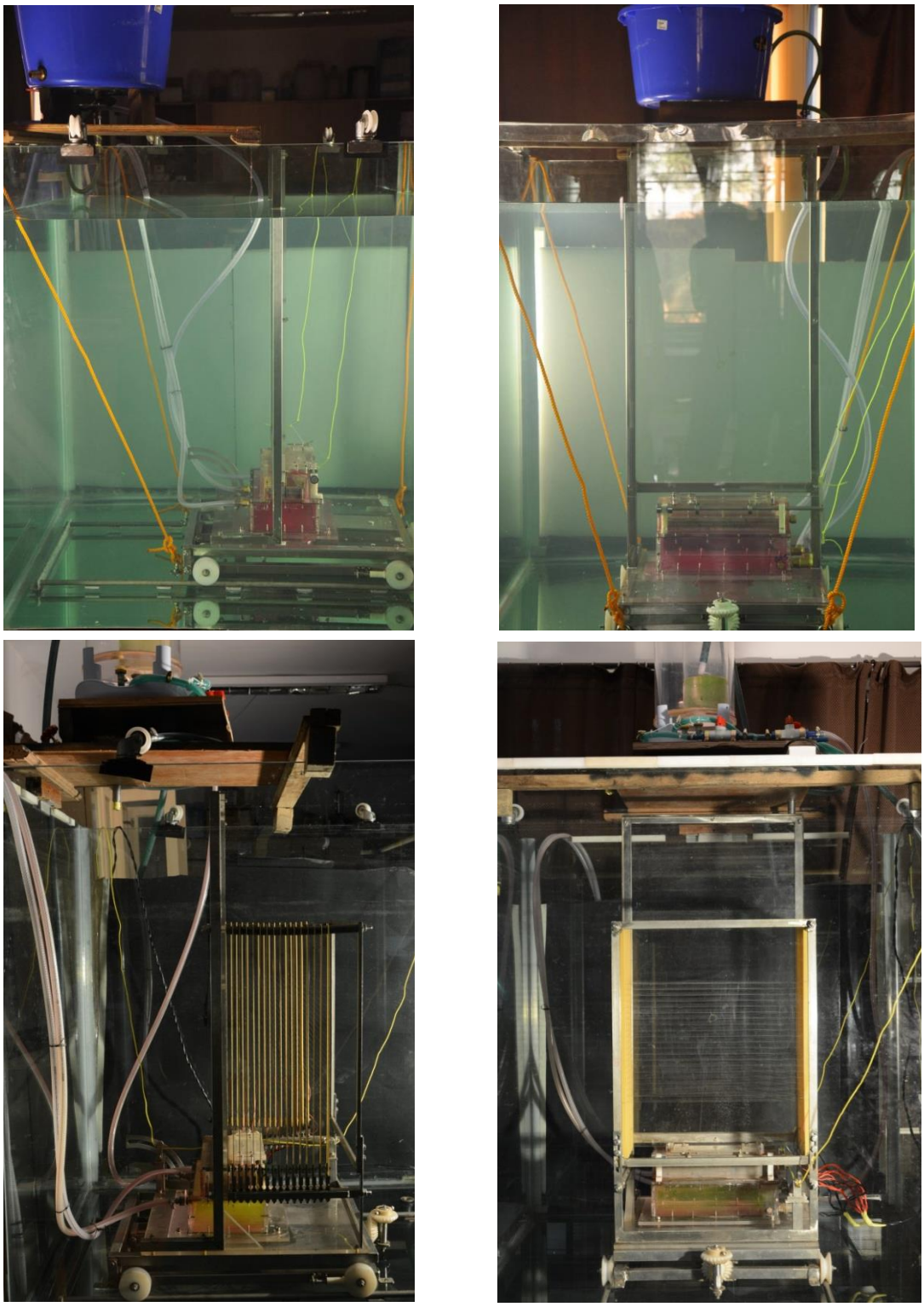

Figure 2.7: Front and Side view of apparatus (a) without heating grid arrangement; and (b) with heating grid arrangement.

The schematic of the apparatus is shown in figure 2.6. The dimensions of the glass walled tank used were 1.2 m × 1.2 m × 1.2 m. The constant head tank was placed at the top of the glass tank. Water was made to continuously overflow to ensure the constant head. The water was drawn from the constant head tank to the settling chamber via piping system. The settling chamber stayed over a base plate. The flow conditioner and the nozzle were placed over the settling chamber to ensure uniform flow at the nozzle exit. The acrylic wall was placed just besides the nozzle exit in such a way that the outlet flow from the nozzle was always tangential to the wall. The wall was made to stand there with the help of a frame which was also fixed to the base plate. There were 17 heating grids placed parallel to the wall with the help of a supporting frame, fixed to the base plate. The base plate was resting over a frame with a screw jack mechanism, so that the complete wall jet apparatus could be inclined, desired to mimic the mountain slope. Figure 2.7 shows the actual image of the experimental apparatus.

2.6.1. Nozzle

In order to produce a planar wall jet, the flow is required to be two dimensional. The initial conditions are also known to effect the development of the plane wall jet downstream of the slot. This study attempted to reproduce the inlet conditions similar to previous two dimensional wall jet studies.

The nozzle with a flow conditioner was designed to ensure two dimensionality of the wall jet, uniform streamwise velocity profile and a low value of turbulence intensity at the slot exit. The exit of the nozzle was a rectangular slot with an aspect ratio 100:1which is large enough for producing a two dimensional wall jet (Launder and Rodi, 1981). Schneider and Goldstein (1994) used aspect ratio of ~90 and Tachie (2000) with aspect ratio of 80 were able to produce two

dimensional wall jets. The width of the slot was 2 mm. The nozzle had a contraction ratio of 46.9. This contraction is known to reduce both lateral and longitudinal velocity variations to a smaller fraction (Mehta and Bradshaw, 1979). Contraction profile used is shown in figure 2.8. A set of four screens at a distance of 10 mm from each other were placed before the nozzle. Screen used was a stainless steel mesh of wire diameter of 1.2 mm with open area ratio of 0.56. The screen is known to remove almost all variations in the longitudinal mean velocity (Mehta and Bradshaw, 1979), thus ensuring uniform flow at the nozzle exit. The drawing for the overall nozzle is shown in figure 2.9.

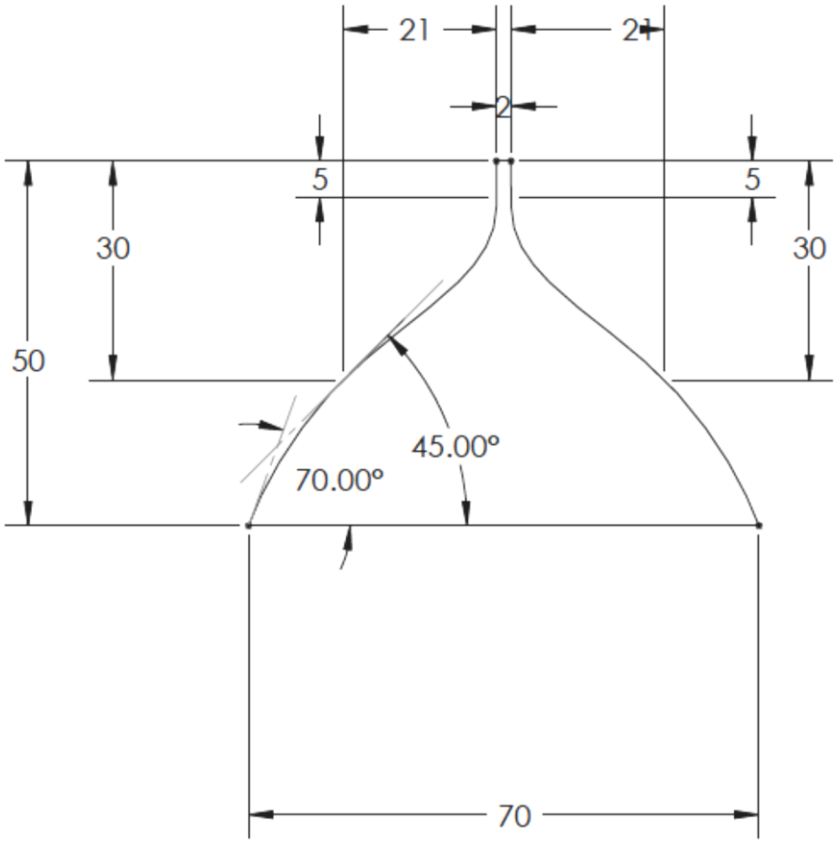

Figure 2.8: Drawing of contraction profile for the nozzle.

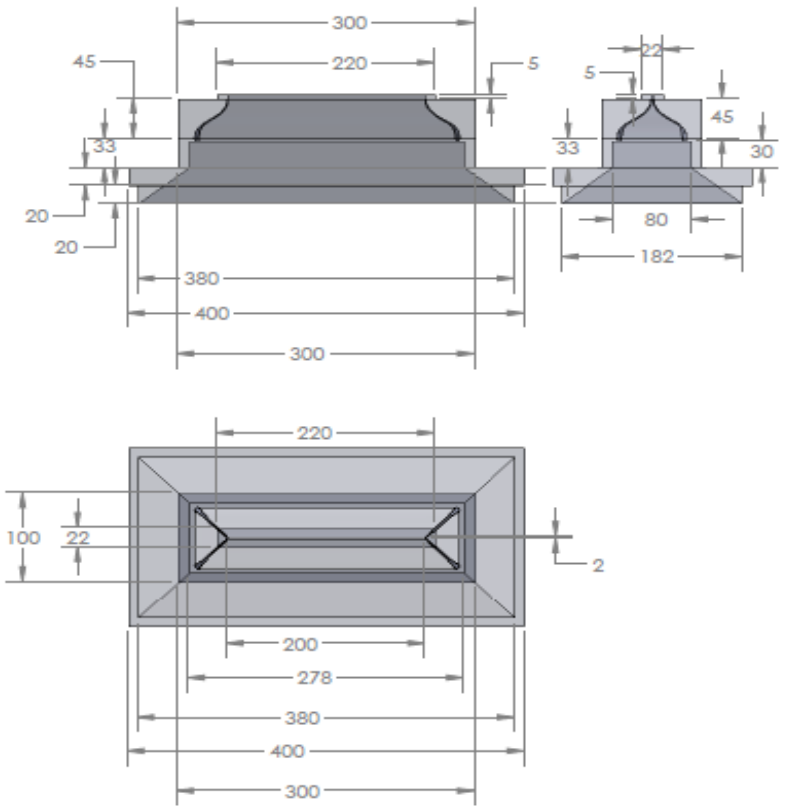

Figure 2.9: Overall drawing of the nozzle.

2.6.2. Heating Grid

Orographic clouds are formed when the moist air mass rises along the mountain slope. After reaching the LCL, the moisture in the air starts condensing. The scattering of light from these water droplets make the cloud visible. But the spreading rate of these clouds is observed to be much lesser than that for the conventional wall jets or wall plumes. As discussed in the earlier part of this chapter the latent heat released due to condensation adds extra buoyancy to the

cloud flow, which results in reduction of entrainment. The mechanism used to mimic the latent heat release in the present study was first described by Bhat et. at. (1989).

The present study basically uses 17 heating grid-elements placed parallel to the wall, with a spacing of 15 mm between each other; the first one touching the wall. The drawing of the heating grid frame is shown in the figure 2.10. All alternate grids were connected together to one terminal of the power source. The flow fluid offered some resistance to the current passage which, in turn, heated the fluid. The ambient fluid was de-ionized water having very large electrical resistance, thus most of the electrical current flows through the jet fluid.

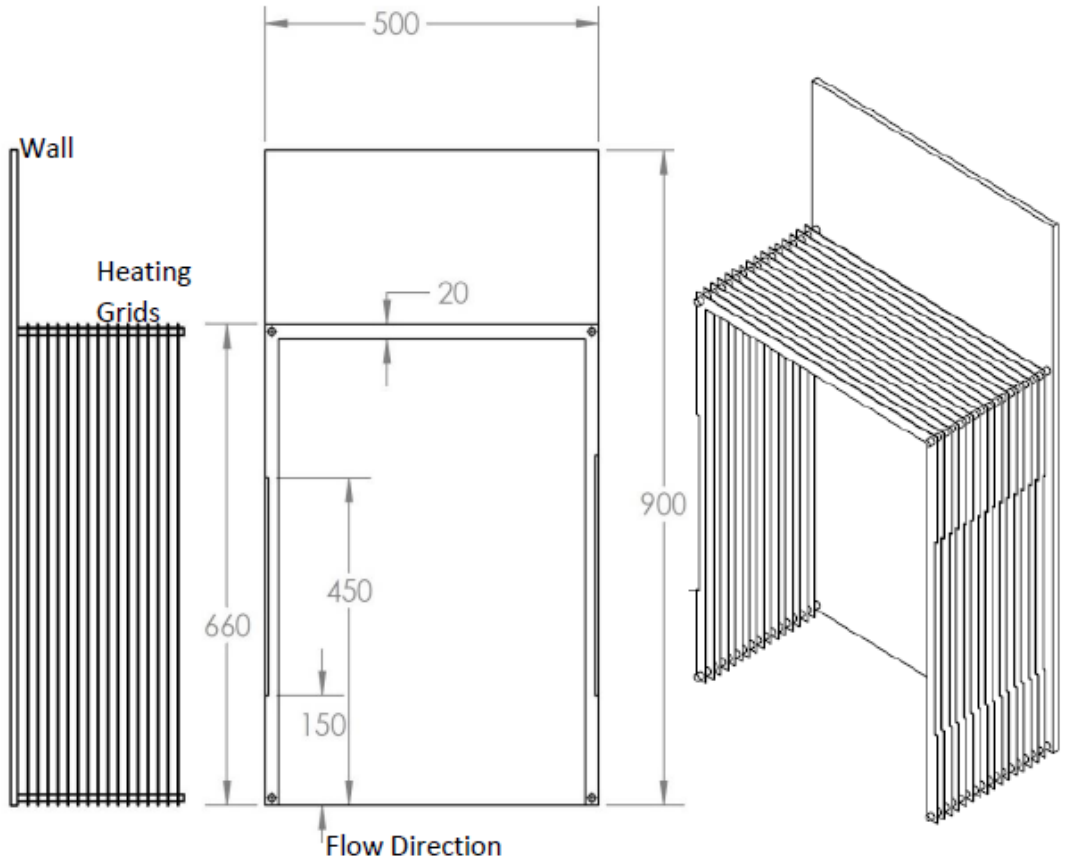

Figure 2.10: Drawing of off source heating grid frame arrangement.

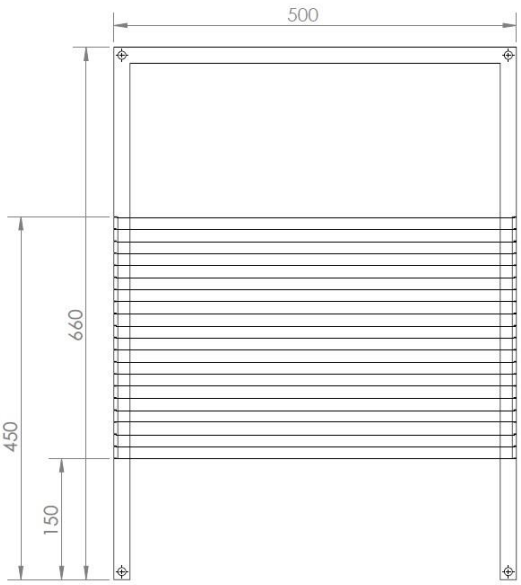

Figure 2.11: Drawing of a single heating grid.

Figure 2.11 shows the drawing of one of the 17 heating grids used. It consists of U shaped strip, having width of 20 mm and 1.5 mm thick. It was held tightly on a SS frame which was fixed to the base plate. The SS wire of diameter of 100 μm was wound around the vertical sides of the U shaped strip starting from 150 mm to 450 mm above the nozzle exit. The vertical distance between two wounded wire strands was 15 mm. The wire Reynolds number was low enough (<10) such that the presence of heating grids had negligible effect on the flow. It was ensured that the heating grids are well insulated from the frame.

2.6.2.1. Problems faced and Solutions

We faced some problems while designing the heating grid arrangement to mimic latent heat released in clouds. The initial design of the heating grid used a U shaped strip made of stainless steel. The wire was wound around this strip frame as discussed previously. All alternate metallic strips were connected to one of the electrode of the power supply (16 kHz variable voltage source). The width of heating grid was 500 mm while the length of nozzle exit was only 200 mm. The idea was that the conducting wall jet fluid, around the middle of heating grid will get heated up because of the current flowing from the wires through the fluid. The fluid around the metallic strips, being nonconductive (deionized water, discussed in next section) would not get heated up. To ensure that there was no current flowing from the top horizontal part of the strips, all strips were coated with insulating varnish. Initial tests in air showed that no current was flowing in the circuit.

But while testing the heating grid in the de-ionized water, to our surprise, we found that there was significant current (~4A for applied voltage of 100V) flowing through the circuit even when there was no conductive jet-fluid coming out from the nozzle exit. After rigorous checking and testing, it was found that the heating grids arrangement was acting as a capacitor. The electrical impedance was considerably low because significant area of the metal strips and reduced distance between the grids compared to that used in other experiments, for example Bhat and Narasimha (1989). The capacitance offered by the set of heating grids was checked by a HTC CM-1500 capacitance meter and was found to be ~12μF with deionized water as the dielectric medium. This value gives an electrical impedance of ~1Ω but it was considerable higher in actual circuit. We were unable to comprehend the reason behind this ambiguity.

Now in order to remove the capacitance effects, the U shaped support metal strips were replaced with similar shaped strips but made of insulating material. The material used was epoxy glass. This material was chosen because of its good electrical insulation properties and high strength which was required to ensure that wires could be wound with sufficient tension. It was found that this new grid arrangement works fine and no current flows through the circuit immersed in de-ionized water and when there was no flow of conductive jet-fluid. The new heating grids had removable top horizontal strip (figure 2.7), further ensuring minimum disturbance to the flow.

2.6.3. Instrumentation

The Nikon D5200 camera with 18-105 mm focal length lens was used for initial dye visualization of the flow. IDT motion pro Y5 (8 GB) was used for the planar laser induced fluorescence (PLIF) imaging of the flow with off source heating. Laser used for this purpose was dual head, Litron Nano L PIV pulse laser with 100 mJ energy per pulse operating at 50 Hz.

The installed deionization plant was used to remove almost all ions from the water in order to make it nonconductive. It was ensured that the deionized water used for experiments had resistivity greater than 14 MΩm. Schematic of working of plant is shown in figure 2.12.

In order to have off source heating of the flow, the heating grids were connected to an external power source. A 16 kHz variable voltage (0 – 240 V) power source from Strayfield Industries was used. 16 kHz power source was used so that there isn't enough resilience time for the water to get vapourized and form bubbles.

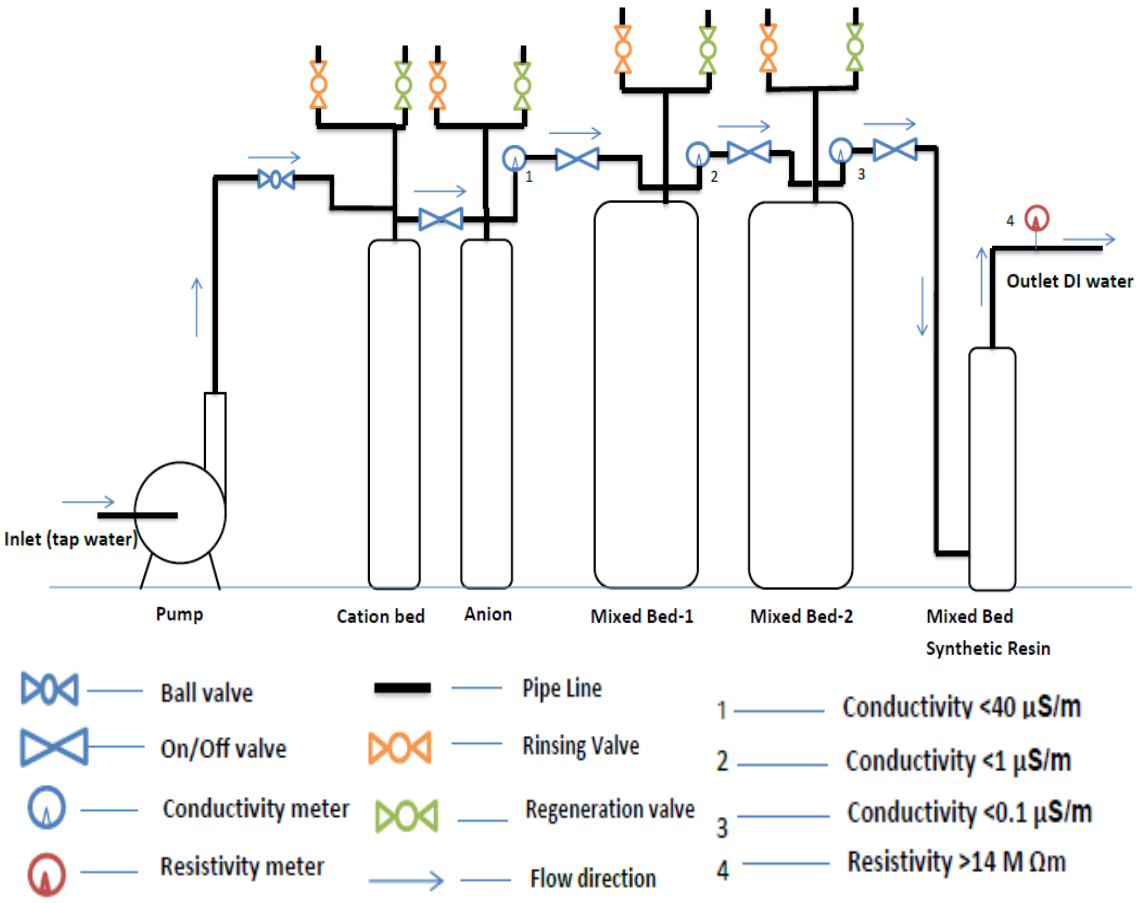

Figure 2.12: Schematic of working of Deionization plant (Supplied by Safewater Technologies, Bangalore)

The density meter, DDM 2911from Rudolph Research Analytical was used to measure the density of the fluids used. It had an accuracy of 0.00005 g/cc.

2.7. The Locally Heated Wall Jet

The glass walled tank was filled with deionized water. The fluid used for wall jet flow was deionized water mixed with NaCl (12 g per litre). The added Na^+ and Cl^- ions made the jet fluid conducting but at the same time made the fluid much denser. So some propan-1-ol, being lighter than water was added to the solution so as to make the resultant solution have the density same as that of deionized water. The heating grids were connected to 16 kHz power source as explained above. The current passed through the ionized wall jet fluid and because of the resistance offered by the fluid to the flow of current, it got heated up. The total heat added to the fluid was calculated using ohm's law, Q = VI where V and I were the voltage and current value shown on digital voltmeter and digital ammeter respectively on the power source.

Reynolds number (Re) of flow in real cloud is $O(10^5)$. This high Re cannot be achieved in laboratory conditions. The Reynolds number in the present study was kept relatively high enough so that the flow is fully turbulent before the heat injection zone. Bhat and Narasimha (1996) proposed a non-dimensional heat release parameter that governs the behavior of cloud-like flows. The non-dimensional number was Bulk Richardson number (G).

$$G \sim \frac{\beta g}{\rho C_p}\frac{Q}{bU^3}$$

$$\sim \frac{Buoyancy\ force\ (due\ to\ heating)}{Initial\ inertial\ force}$$

where β is thermal coefficient of expansion of cloud fluid, g is acceleration due to gravity, ρ is the density of ambient fluid, C_p is specific heat at constant pressure of ambient fluid, b and U are length scale and velocity scale and Q is the off source

heating rate.In the present experiment, this non dimensional number was matched with that in real clouds to have dynamical similarity.

For cumulus clouds, G is in the range of 0.1 – 2 while for cumulonimbus clouds it varies from 0.3 – 3 (Venkatakrishnan *et al.*, 1999). Because of lack of data on orographic clouds, Bulk Richardson number for such clouds in unknown. The heating rate, Q in the experiments presented was adjusted accordingly in order to have G within this range (assuming G for orographic clouds is of the same order as that for free standing convective clouds).

2.8. Experiments

2.8.1. Preliminary Dye Visualization without off source heating

The initial set of experiments was to just quantitatively visualize the wall jet without any off source heating. Dye visualization of wall jet was performed using Aludine Red dye. Aludine was mixed with conductive water solution and some more propan-1-ol was added to have the solution density same as before. Figure 2.13 shows the development of the wall jet at Re ≈ 1500.

This experiment was just to demonstrate the apparatus and check if apparatus was working fine. Figure 2.13 demonstrates the wall jet developing vertically. The apparatus was designed in a way that it could be inclined at some known angle. Figure 2.14 shows the side and front view of the wall jet development at an inclination of 25^0 with vertical.

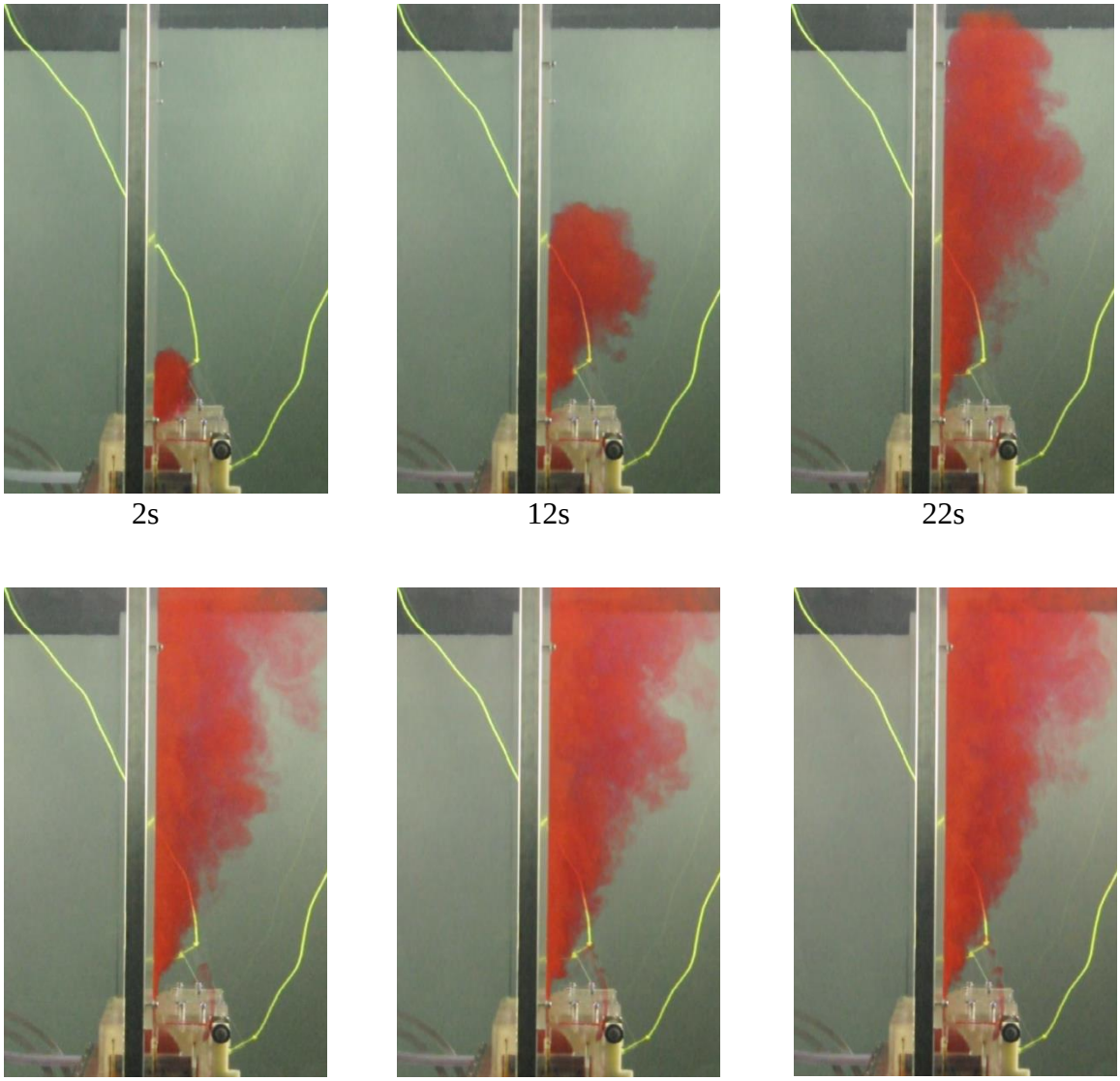

Figure 2.13: Development of wall jet (Re≈1500).

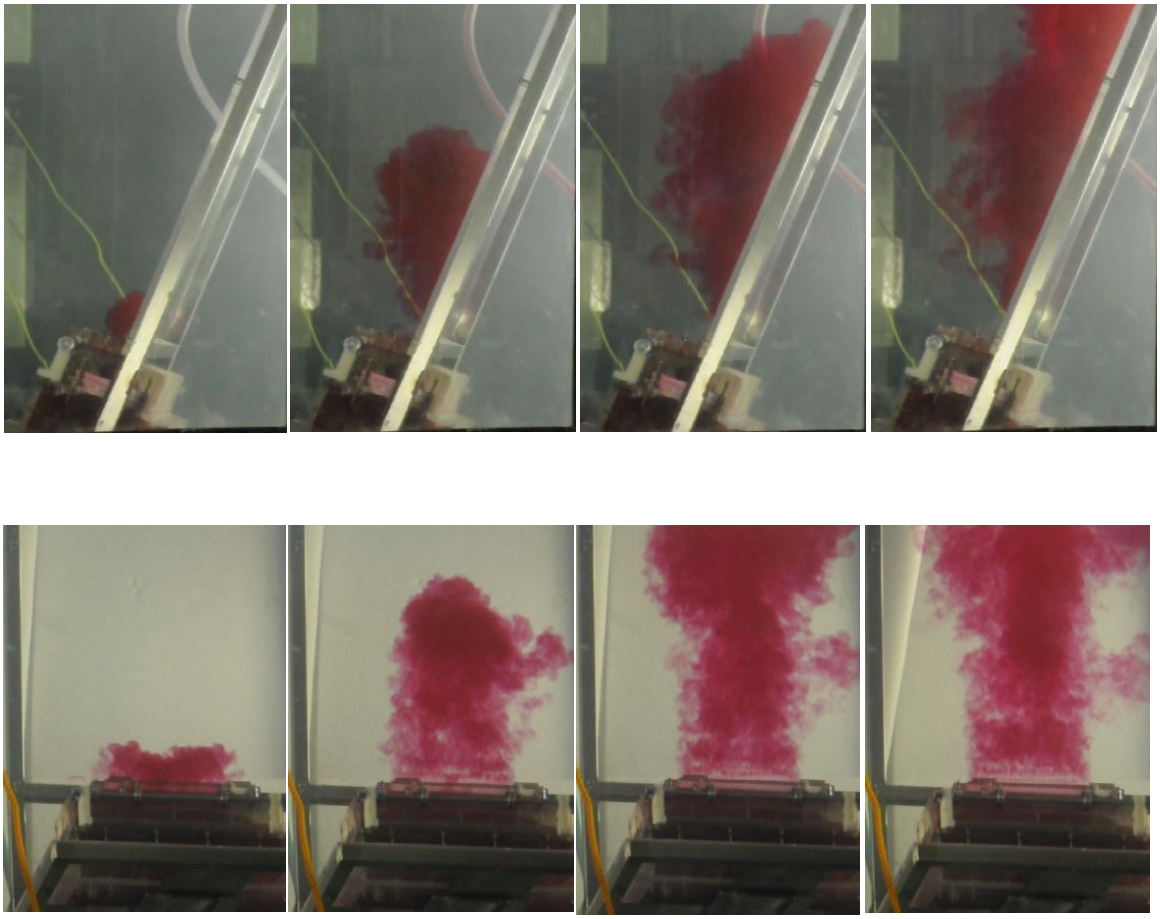

Figure 2.14: Development of wall jet inclined at 25^0 with vertical (side view and front view) (Re≈1500).

2.8.2. PLIF visualization with off source heating

The PLIF experiment was performed for a steady wall jet. The Reynolds number was ~1500. The flow was allowed to reach steady state before camera was triggered. The dye used was Rhodamine 6G.

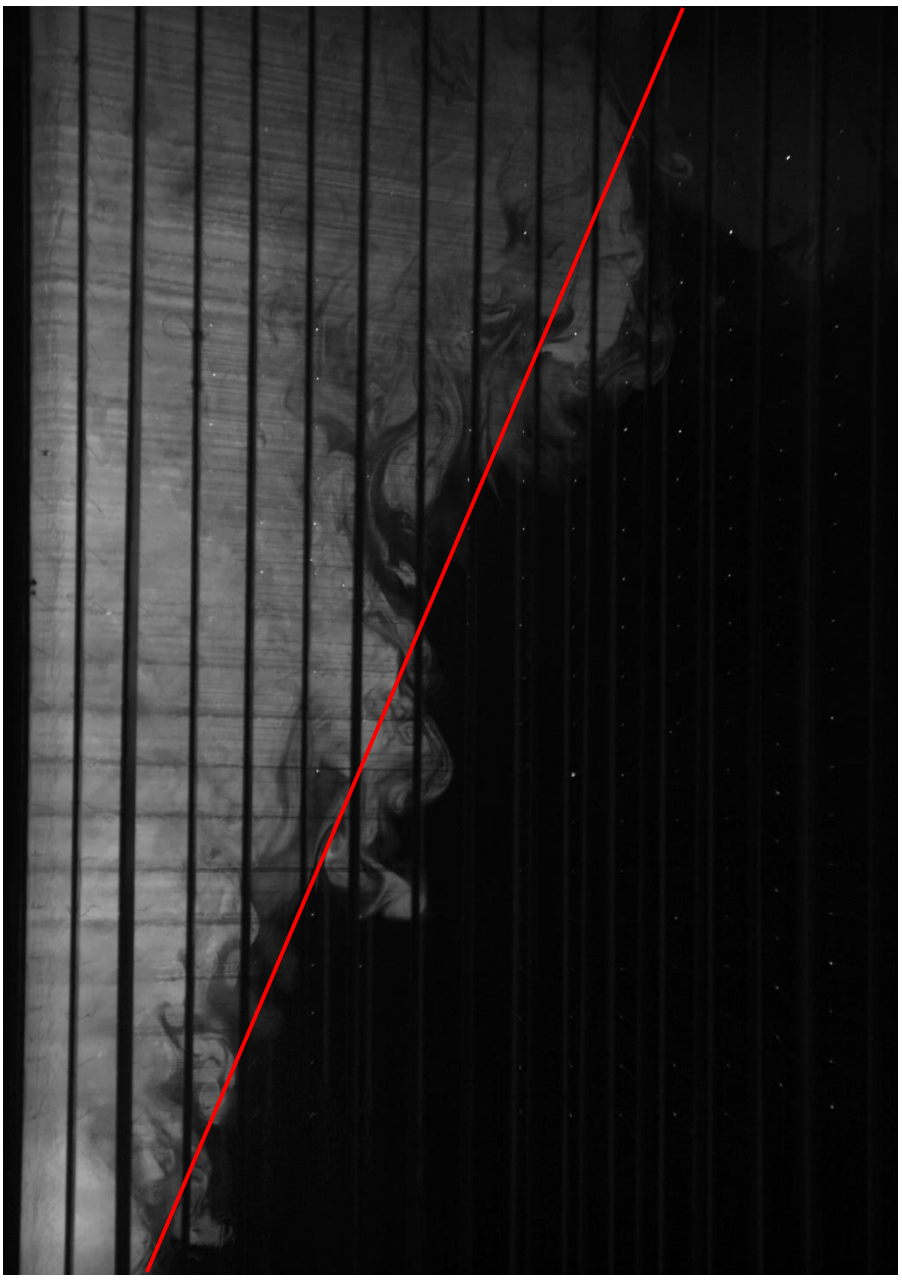

Figure 2.15: Instantaneous image of steady wall jet without heating.

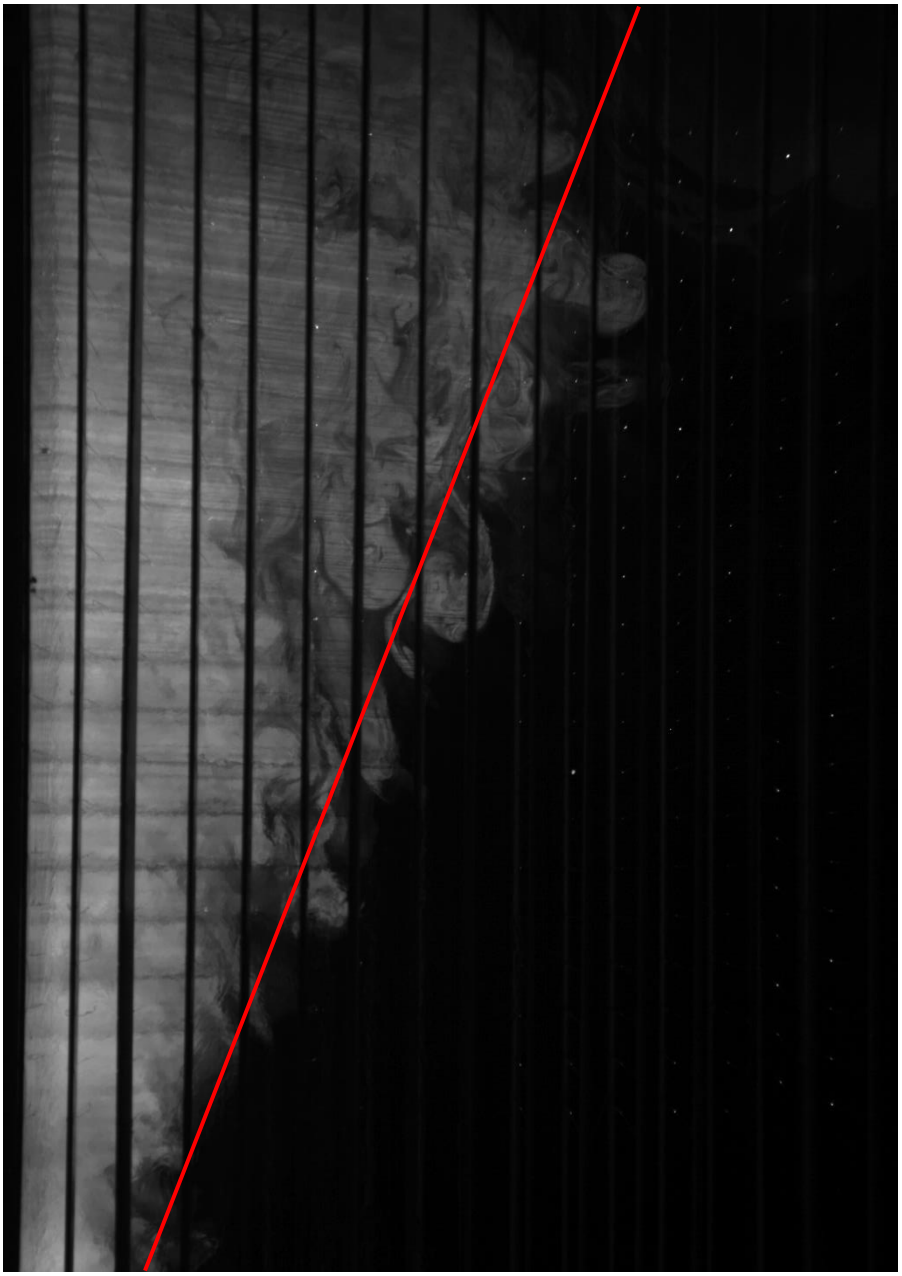

Figure 2.16: Instantaneous image of wall jet with off source heating (100V and 3.9A).

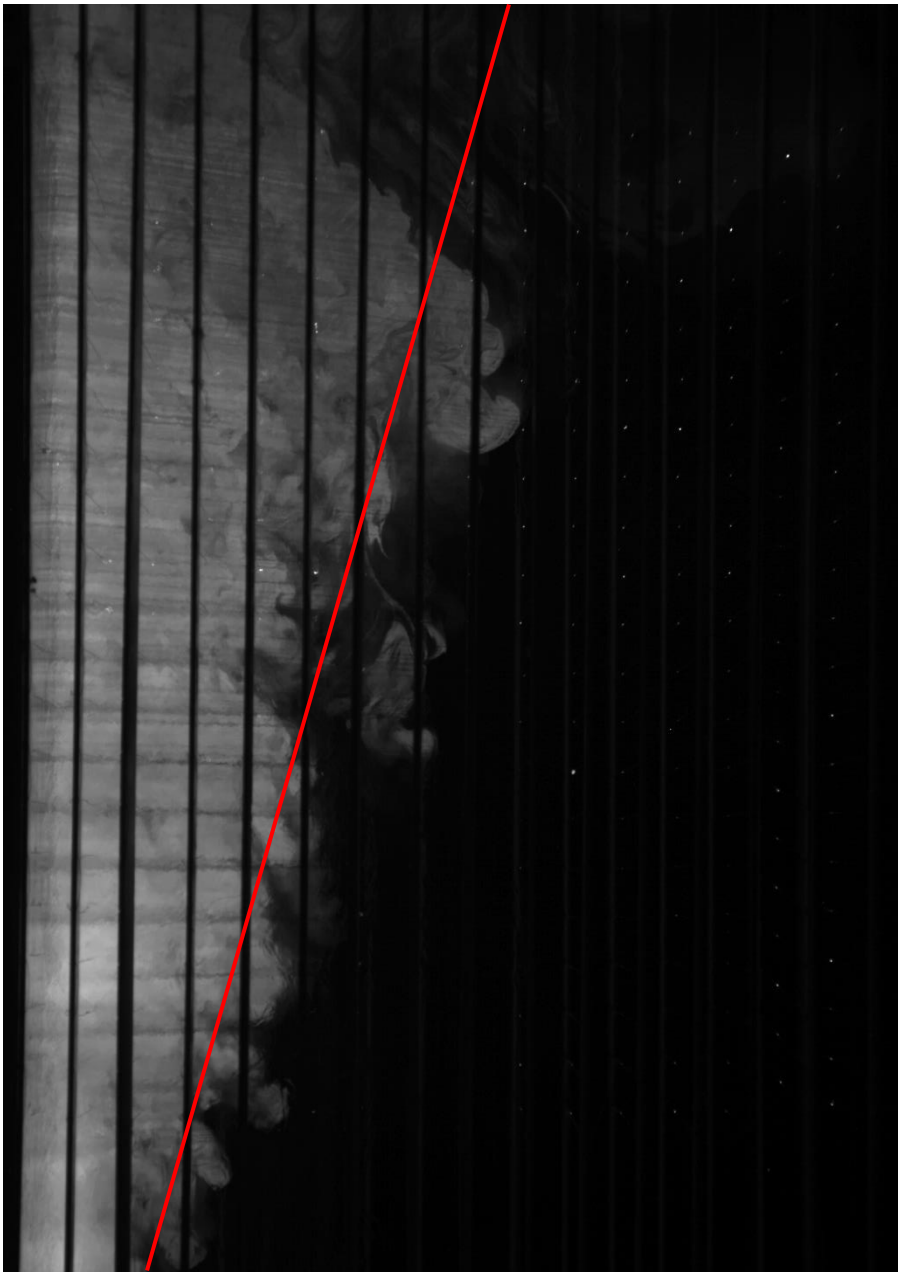

Figure 2.17: Instantaneous image of wall jet with off source heating (200V and 7.2A).

Figure 2.15 shows the instantaneous image of wall jet after achieving the steady state. Actual physical dimensions of the image are 380 mm * 240 mm. Vertical dark lines seen in the image are the epoxy glass strips. Red line was drawn to approximately mark the edge. When voltage was applied, the entrainment started to reduce. Figure 2.16 show the image 10 seconds after the voltage of 100V was applied. The current drawn was around 3.9A. Now marking an approximate edge showed some reduced width (although very little) which could be attributed to reduced entrainment. The voltage was further increased to 200 V and current drawn was around 7.2 A. Figure 2.17 shows the image 10 seconds after the voltage was increased. Here the width was seen to have decreased significantly and this became more evident after drawing the red approximate edge line.

2.9. Results and Discussions

It was seen that as the amount of heat added increases, the width of the wall jet decreases. It could be the reduction in the ambient fluid getting engulfed into the turbulent region. This could be seen in figures 2.15, 2.16 and 2.17. We can see that the area of dark patches in turbulent region was highest for non-heated wall jet which keeps on decreasing as the heating rate is increased.

As seen in figure 2.17, the entrainment reduces drastically when applied voltage was increased to 200 V. The heat addition rate was ~1.4 KW over the volume greater than 3000 cm^3 which implies that the heat addition rate per unit volume was less than 0.5 MW/m^3. This value is much lesser than that used by Narasimha *et al.* in their experiments. There could be two possibilities behind this anomaly:

1. In our experiment, the placement of heating grids was different. Those were placed parallel to the direction of mean flow. The heat addition near the wall was greater than that around the edges because of more concentration of conductive fluid near the wall. This might have resulted in drastic reduction in entrainment.
2. It is some inherent phenomenon related to wall jets that even a little heat addition results in drastic reduction in entrainment. This is consistent with some of the orographic clouds photographs (figure 2.3, 2.18) found over the internet. It could be seen in these photographs that the width of the orographic cloud is very less, even on inclined slopes where natural tendency of buoyant cloud (because of latent heat release) is to spread upwards.

Figure 2.18: (a) Orographic clouds surrounding Mount Oltar peak (Image Credits: Stefano Zerauschek, Source: Flickr) (b) Orographic clouds develop across massif (Image Credits: Roddy Addington, Webpage:roddyaddingtonphotos.zenfolio.com)

Based on the present study, no conclusive comment could be made regarding entrainment anomaly. More experiments are required to properly understand the phenomenon.

CHAPTER 3

STUDY OF JET USING LASER INDUCED FLUORESCENCE BASED TOMOGRAPHY

3.1. Introduction

Turbulent mixing of passive scalar is very important in many environmental flows. Formulation of many such problems is possible, in terms of mixing of dynamically passive and conserved scalar quantity. Distribution of salinity or organic matter in oceans and dispersion of effluents in the atmosphere from a chimney are some such examples. Cloud is another example where understanding turbulent mixing is very important. In clouds, water droplets are formed during condensation, which chiefly depends on the mixing of dry air and the water vapour in the rising air-parcel. Thus the measure of scalar mixing in a cloud-like flow could give an idea of water droplet distribution in a cloud. The main objective of this experiment is to study the dilution rate of a scalar both spatially and temporally in turbulent shear flows.

Earlier, this was done by adding some passive chemical tracer in the flow and measuring its concentration at different points in the flow using probes. Roberts *et al.* (2001) used conductivity probes to measure salt tracer concentration in water. The problem with these techniques was the limited spatial resolution. Advent of laser induced fluorescence (LIF) technique allowed us to capture two dimensional concentration fields. In this technique, a fluorescent dye was used as a tracer in the flow and the laser sheet was used to illuminate a plane of the flow. In the dilute concentration of the dye, fluoresce light emitted from the dye is proportional to concentration of the dye in that region and can be used to quantify mixing. Many studies using LIF have been reported previously, for example, Dimotakis *et al.* (1983), Prasad and Sreenivasan (1990) and Venkatakrishnan *et al.* (1998). But the

turbulent mixing, even in the simplest flows is inherently three dimensional. Thus, using two-dimensional planar images to quantify entrainment and mixing would be difficult and in some scenarios misleading.

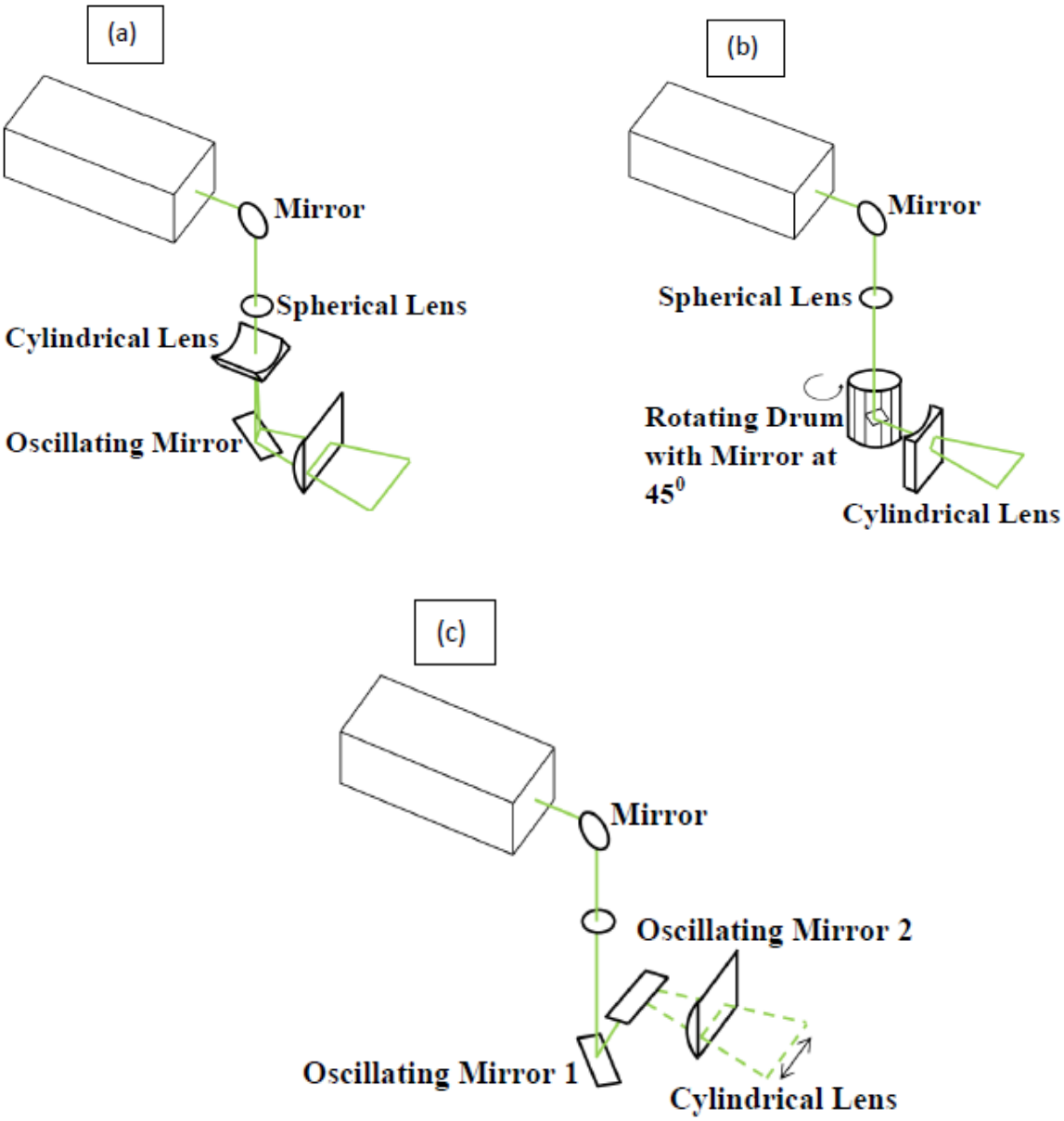

Figure 3.1: Schematic for optical arrangement for sweeping laser sheet (a) using oscillating mirror, (b) using rotating drum and (c) using a set of two oscillating mirrors.

To measure the dilution in whole field, three dimensional LIF was introduced where the laser sheet was made to sweep across the flow field at high speed and images of 2D concentration field were recorded at various sections (for example, Tian and Roberts, 2003). The idea was to sweep through the flow flied at fast enough speed so that flow could be assumed as 'frozen'. These two dimensional images were then reconstructed to get a three dimensional concentration field.

A cylindrical lens was used to expand laser beam into a sheet. Most of the experiments till date use either one of the three optical arrangements, as shown in the figure 3.1, to sweep the laser sheet through the flow field. The most commonly used optical arrangement for sweeping the laser sheet is using an oscillating mirror driven by a galvanometer (figure 3.1 (a)). This system cannot produce parallel sheets. So to simplify post processing, the flow apparatus is kept a little far away so that the sheets at different sections could be assumed parallel or use another cylindrical convex lens to ensure that all sheets are parallel. Prasad and Sreenivasan (1990), Merkel *et al.* (1996) and Ruck and Pavloski (2000) used this kind of configuration. The rotating drum configuration consists of a circular cross section drum with small mirrors attached around the circumference (figure 3.1 (b)) in a helical pattern at equal intervals to achieve sweeping of the laser sheet in vertical direction. The mirrors were inclined at 45^0 to the rotation axis so that the laser sheets are always perpendicular to the axis. The drum was made to rotate at constant angular velocity (figure 3.1 (b)). Guezennec *et al.* (1994) and Delo and Smiths (1997) used this method to sweep laser sheet across the flow field. Some studies like Patrie *et al.* (1994) used similar rotating scanner with parabolic mirror so that intensity distribution was same along the width of the section. Dahm *et al.* (1991) devised a new technique to have uniform laser intensity laterally which helped in easy extraction of tracer information. They used two galvanometer oscillating mirrors with axis orthogonal to each other to sweep the laser beam in a raster scan fashion through the flow volume. However, the swept sections were

not parallel to each other. Tian and Roberts (2003) used same technique and placed a convex lens in front to have parallel scan sections (figure 3.1 (c)). Using this combination they were able to scan much larger volume of the flow.

There is some deficiency in all the above mentioned configurations. In all cases, the flow volume which could be scanned is limited. In oscillating mirror configurations, it is limited by the size of the convex lens. Getting a big lens fabricated for this configuration is costly and also is not readily available. Synchronizing the galvanometers and the camera is another difficult task as well. Necessity of a good PLC for controlling the galvanometer precisely will further increase the cost of the system. Also it is almost impossible to get precisely parallel sheets, thereby always having some inherent error in the measurement. In the rotating drum system, however the sheet is always parallel but the height of the volume scanned is very much limited by the size of the drum and the length of the diverging lens.

In the present study, we report a technique to sweep the laser sheet through the flow, while ensuring sheet is always parallel and using conventional readily available optics. The overall scanning system is extremely cost effective. We used this new 3D LIF technique for imaging a round jet. This flow was chosen because of vast literature available to compare with, and later relate this to cloud type flows.

3.2. Jets in a homogenous environment

An unbounded region of a large body of fluid that either has an excess momentum or a momentum deficit is a free shear flow (figure 3.2). Jets (driven by initial momentum), plumes (driven by initial buoyancy), wakes (characterized by initial momentum deficit) and a mixing layer (characterized by velocity difference across the interface of two co-flowing fluids), all are examples for free shear flows. A free shear flow, during its development along downstream flow direction induces the irrotational ambient fluid to get into and mix with the turbulent flow. This process of bringing in and mixing of ambient fluid into the free shear flows is known as 'entrainment'. The hypothesis for the mechanism of entrainment was first given by Sir GI Taylor in a wartime report (Taylor, 1946). The entrainment hypothesis in its original form can be stated as "the mean inflow velocity across the edge of a turbulent flow is assumed to be proportional to a characteristic velocity, usually the local time-averaged maximum mean velocity or the mean velocity over the cross-section at the level of inflow" (Turner, 1986).

Figure 3.2: Free shear flows. (a) Jet (b) Wake (c) Mixing layer (Blue line shows the velocity profile for each case). (Manikandan, 2005)

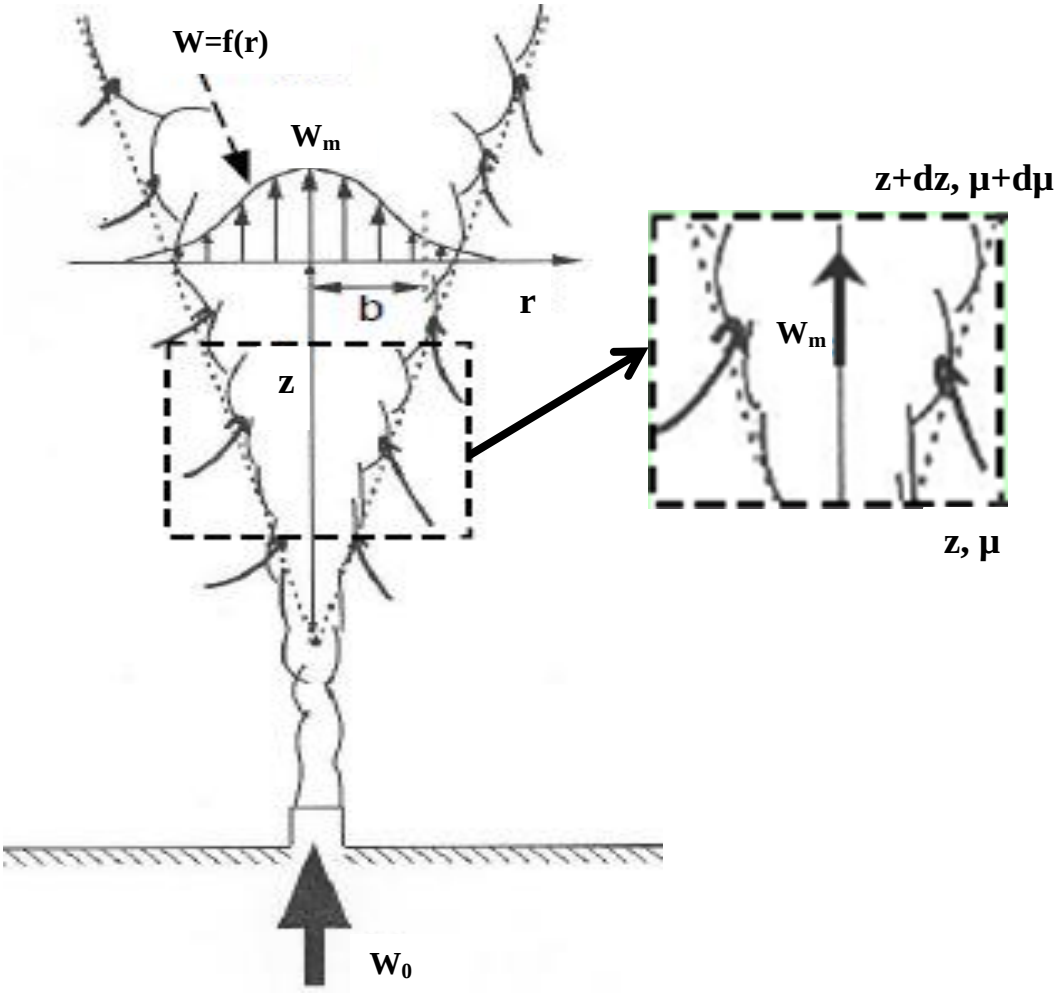

Figure 3.3: Typical entrainment process in a jet. (Manikandan, 2005)

For a steady axisymmetric round jet, the two basic integral properties, mass and momentum flux, are defined as:

$$\rho\mu = 2\pi \int_0^\infty \rho w r dr$$

$$\rho m = 2\pi \int_0^\infty \rho w^2 r dr$$

where ρ is the density of the fluid, μ is the specific mass flux or volume flux, m is the specific momentum flux and w is the local mean vertical velocity at a distance r from the centerline.

A pure jet is defined by total momentum (M) alone at its origin, since M remains constant at all stream-wise locations. The time averaged mean vertical velocity profile is self-similar, and is described well by a Gaussian profile.

$$W = W_m exp\left[-\left(\frac{r}{b_w}\right)^2\right]$$

where W_m is the mean vertical velocity at the centerline and b_w is the characteristic radial scale for velocity. A passive scalar spreading through its initial flux, also shows similar time averaged concentration profile.

$$\theta = \theta_m exp\left[-\left(\frac{r}{b_\theta}\right)^2\right]$$

where θ_m is the mean centerline passive scalar concentration profile.

It is possible to deduce almost all properties of turbulent jets using dimensional arguments combined with empirical data (Fischer *et al.*, 1979).

$$W_m = (7.0 \pm 0.1) l_Q M Q^{-1} z^{-1}$$

$$\theta_m = (5.6 \pm 0.1) l_Q \theta_0 z^{-1}$$

$$\mu = (0.25 \pm 0.01) {l_Q}^{-1} Q\ z$$

$$b_w = (0.107 \pm 0.003)\ \mathrm{z}$$

$$b_\theta = (0.127 \pm 0.004)\ \mathrm{z}$$

where M is the initial specific momentum flux, Q is the initial volume flux and $l_Q = \sqrt{A}$, A being the cross sectional area of the nozzle exit. $b_w$and b_θ are the jet

half widths (that is the distance from the centre where the value reduces to half of the maximum value) for velocity and passive scalar respectively. The ratio b_w/b_θ(=1.2) is a constant.

It follows from the above equations that:

$$\mu \propto wb^2 \propto M^{\frac{1}{2}} z$$

$$\frac{d\mu}{dz} = constant$$

Now taking into account the entrainment assumption i.e. the inflow velocity at any level at the 'edge' of the flow is some fraction α of the maximum vertical mean velocity at that level. α, is also known as entrainment coefficient. Using this notation, it implies:

$$\frac{d\mu}{dz} = 2\pi b_w \alpha W_m$$

The equations for conservation of mass and momentum for a jet can be written as:

$$\frac{d}{dz}\left({b_w}^2 W_m\right) = 2\alpha b_w W_m$$

$$\frac{d}{dz}\left(\frac{1}{2}{b_w}^2 {W_m}^2\right) = \lambda^2 {b_w}^2 g\theta_m$$

For a detailed discussion on derivation and underlying assumptions refer Turner (1973). Fischer *et al.* (1979) have used experimentally determined parameters to show that (for Gaussian profiles)

$$\alpha_{Jets} = 0.054$$

The value of α given above is only indirectly related to the angle of spread of velocity profile in jets. For jets, $db_w/dz = 2\alpha = 0.107$, as already set out using dimensional argument.

3.3. Experimental Setup

The Schematic of the experimental facility is shown in figure 3.4. The setup consists of a square cross section tank having width of 0.5m and height of 0.8m. A glass blown nozzle with exit diameter of 2mm was used to produce the jet. The distance of 125d from the nozzle to the tank wall was large enough so that the wall effects are negligible. An acrylic stand was fabricated to place this nozzle at the bottom of the tank. An overhead tank was used to supply fluid to the nozzle with some head. The fluid was made to continuously overflow from the overhead tank to ensure fluid was supplied at constant head to the nozzle. This was achieved by placing a cylindrical pipe inside another cylindrical pipe of bigger diameter. The fluid from the outer annular space was continuously pumped into the inner pipe using a submersible pump. The piping system was fitted with valves so that the flow rate could be controlled.

For the three dimensional LIF, an optical arrangement was designed capable of scanning large volume and producing completely parallel laser sheets at all sections. The laser beam was made to fall normally on the face of a right angle prism which made the beam to turn by 90 degrees. Next a combination of spherical convex lens and concave cylindrical lens was used to produce a laser light-sheet. Now the set of prism, spherical lens and cylindrical lens was placed on the top of a carriage of a linear actuator. The carriage was made to move to and fro by a frictionless ball screw arrangement which was driven by a servo motor and drive-system. The drive was controlled using a single axis PLC. The carriage was made to move for a known distance at constant speed, thereby ensuring that the sheet is always parallel. A high speed camera was used to capture images. All the optics and other components used here are the conventional readily available ones, which made our technique very cost effective.

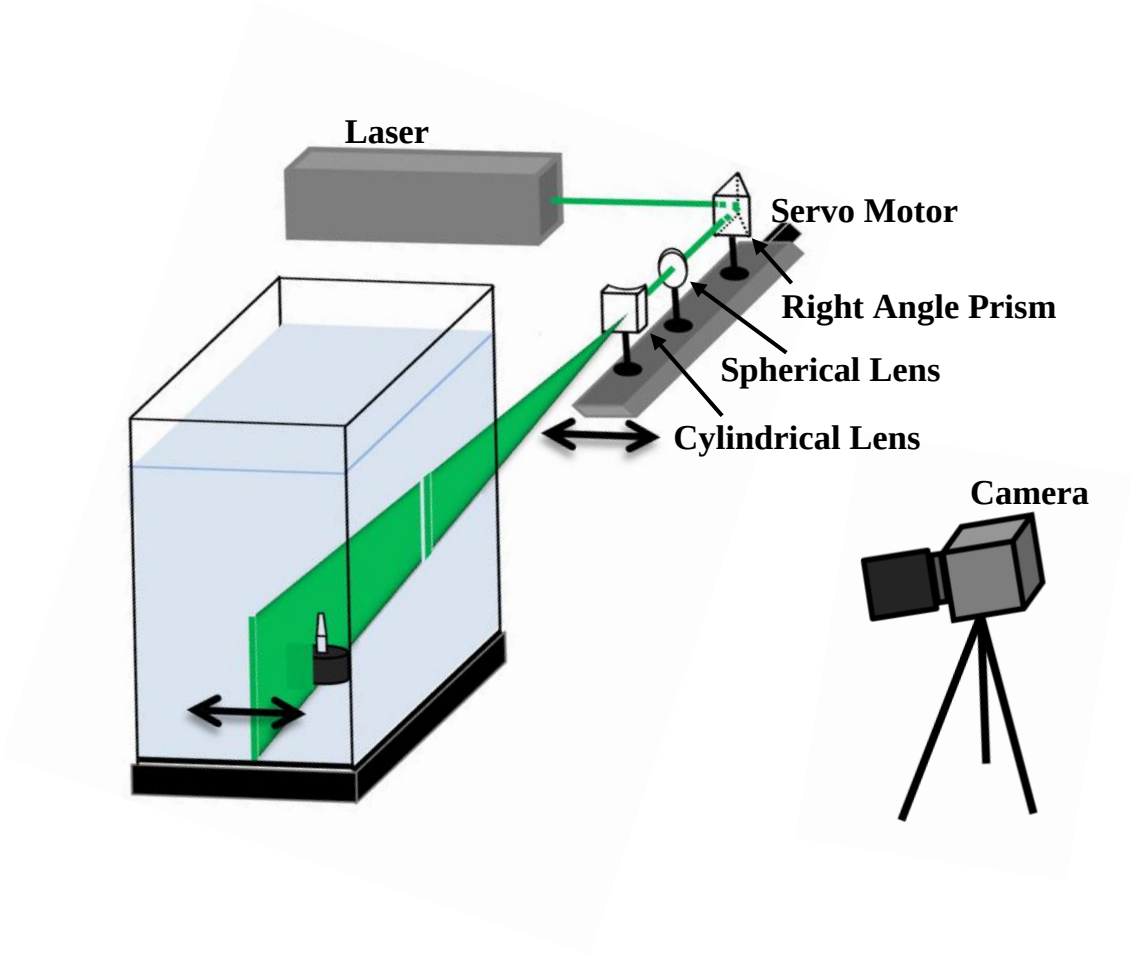

Figure 3.4 (a): Schematic of experimental setup.

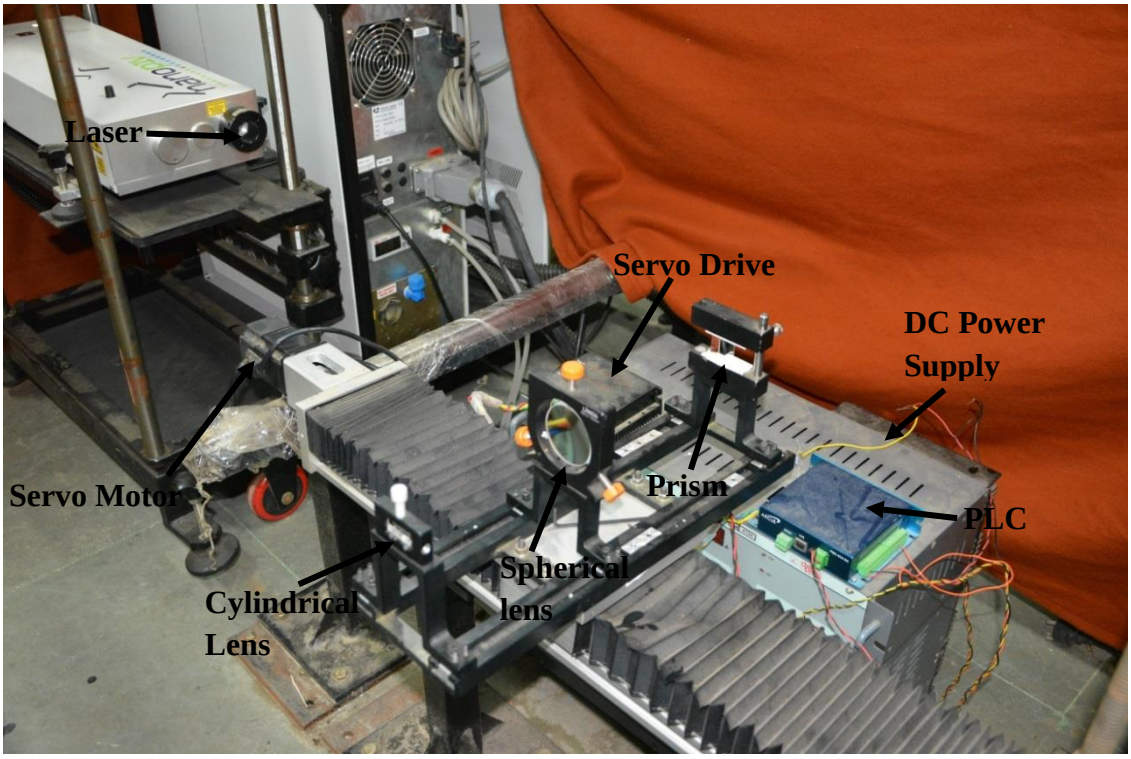

Figure 3.4 (b): Actual image of laser scanning setup.

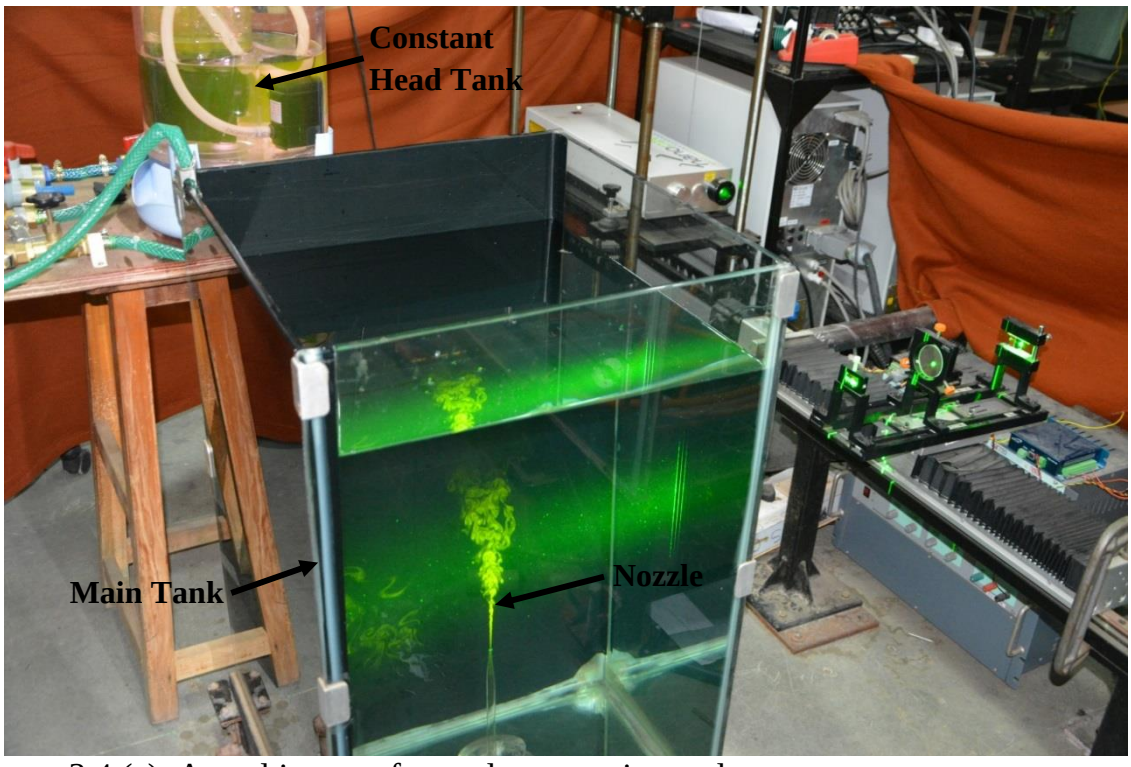

Figure 3.4 (c): Actual image of complete experimental apparatus.

3.3.1. Other details about the setup:

The laser used was Litron Nano PIV dual head Nd:YAG pulse laser (532 nm) with specification of 100 mJ per pulse with a pulse duration of 4ns and each head capable of pulsing at maximum of 50 Hz. Each head was made to pulse at 50 Hz with the delay between two heads arranged such that, we got 10 ms separation between pulses illuminating the flow. In order to have this delay setting, the two laser heads were synchronized and trigged using Stanford digital delay generator, model DG645. Overall two-laser heads put together was pulsing at 100 Hz frequency with 10ms time separation between light pulses. The camera used was an IDT Motionpro Y5. 70-300 mm focal length Sigma lens was used to focus the light onto the camera sensor. The optics used were (a) a right angle prism with 25 mm edge and 25 mm height, (b) a 500 mm focal length and 50 mm diameter plano-convex spherical lens and (c) a sheet shaping cylindrical plano-concave lens of 12.5 mm focal length and size of 12.5 mm *25 mm. All these optics were readily available. This set of optics was placed on the carriage of the ball screw linear actuator, MAX 124 BLC – 500 mm stroke from Maxima motion and Control Pvt. Ltd. The schematic of linear actuator is shown in figure 3.5. The servo motor and servo drive system was used to drive the linear actuator. A 200W AC servo motor JMC 60ASM200 with 2500 lines/revolution encoder resolution and a digital AC servo driver, JMC MCAC506 was used. A standalone PLC controller, Arcus PMX-4CX-SA was used to give inputs to the driver.

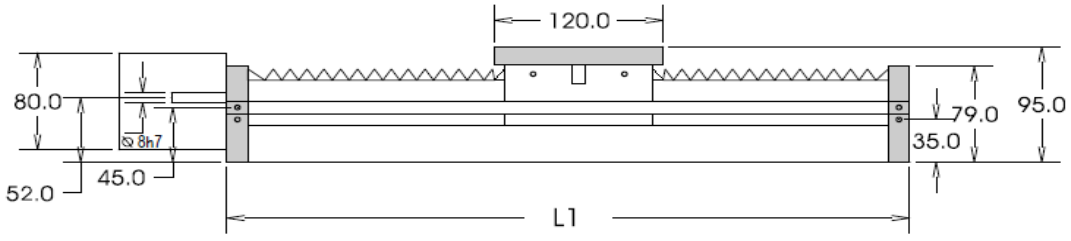

Figure 3.5: Schematic of linear actuator. (L1=500mm). (Taken from manual)

3.4. Experiments - Methodology

As mentioned before, we used the new 3D LIF technique for imaging jet flow in quiescent surrounding. The main tank and the overhead tank were filled with clean water. The nozzle was kept at the bottom of the tank. The height of the nozzle exit from the bottom of the tank was 25 cm. Around 400 µg/L of Rhodamine 6G was added to the overhead tank, thereby ensuring a linear relationship between concentration and intensity (Shan et. al, 2004). Rhodamine 6G absorption spectrum peaks for 530 nm wavelength of incident light and its emission range is 555 nm to 585 nm with a maximum at 566 nm. So in order to block the spurious scattering and other effects from the 532 nm incident light, an OD4 longpass filter with transmission range of 560 – 1650 nm was used. The camera was placed at a distance of 4 m from the tank. The lens was used at its maximum focal length of 300 mm and F number of 5.6. This configuration was used in order to have a low viewing angle, so that the change in magnification from front to end of the scanning volume was less. Also this ensured that variation in attenuation coefficient for the light at different sections across the volume was negligible. The camera was focused on the centre plane but the images obtained off this plane might have been completely out of focus but placing the camera at a large distance from the tank also ensured that there is minimal defocusing for the off centre planes. However, defocusing was also tested by obtaining images of some test pattern at various distances without refocusing. It was found that images remained in acceptable focus at least up to ± 75 mm from the centre plane, which was within our region of interest (figure3.6). Another advantage of this configuration was that the assumption of laser sheet is perpendicular to camera comes out to be handy as any minor deviations will have negligible effect. Although effort was made to ensure that camera was placed perpendicular to the plane of laser sheet.

(a) 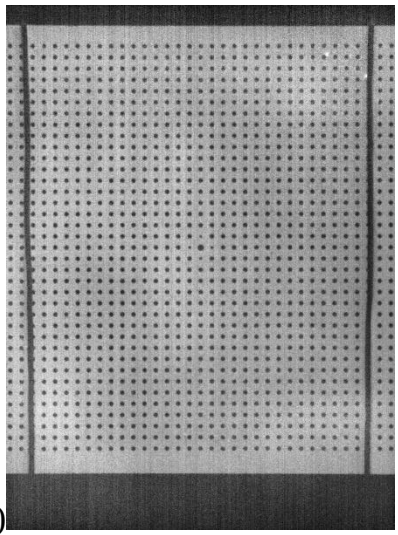 (b) 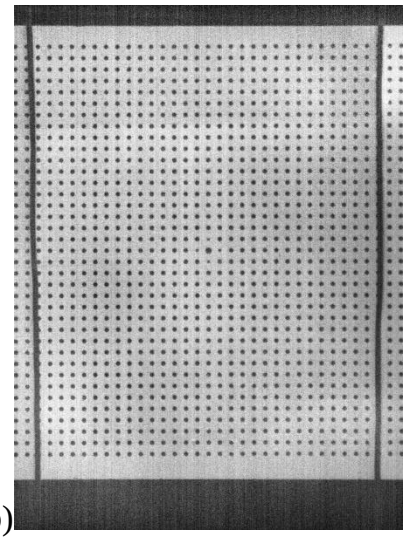

(c) 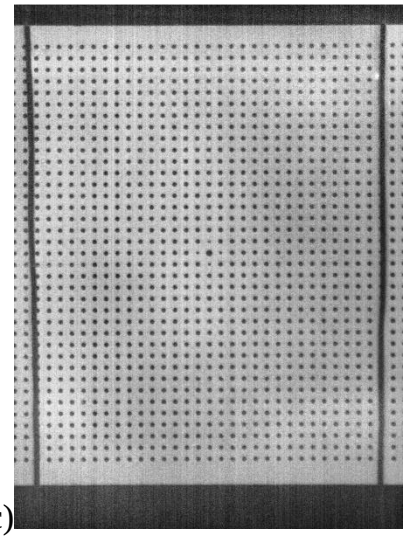

Figure 3.6: Estimation of defocusing and change of magnification using a calibration plate at (a) the plane 75 mm behind the centre plane, (b) the centre plane and (c) the plane 75 mm in front the centre plane.

The laser had to be aligned such that the laser beam was always perpendicular to one of the right angled face of the prism. This was done by manually moving the actuator forward and backward and adjusting the laser such that the laser beam always hits the prism at the same location. The PLC was programmed in order to

make the linear actuator move a total distance of 140 mm in a time period of 1000 ms with duration of 10 ms in the beginning and ending for acceleration and deceleration respectively. The camera was made to capture images at rate of 100 frames per second. This implied that the distance between two planes was ~1.41 mm. The laser sheet thickness was ~1 mm which meant that the camera captured almost the complete three dimensional concentration field of the jet in one scan.

3.5. Calibration and Corrections

The camera was placed at a distance of 4m from the tank. This configuration had few advantages as mentioned earlier, but there were few disadvantages as well. The light intensity follows the inverse square law. Therefore the intensity of light reaching the camera was reduced considerably which meant signal to noise ratio was low. But at the same time, difference in intensities of light reaching the camera from different planes was negligible. Secondly, although the viewing angle for the camera was low, but still there was some change in magnification as laser sheet moves from front to back plane, which meant each plane had different geometric scale (cm/pixel). A test pattern with known dimensions (figure3.6) was used to check the geometric scale at different sections.

Figure 3.7 shows the greyscale level image obtained by covering the lens. For a perfect camera sensor, this image would have been uniform. It was also seen that for the images of the uniformly painted white wall, the intensity value was higher at the center and lower near the edges. This phenomenon is known as ‘vignetting’. Attenuation of the laser sheet intensity along the width of the tank was significant as well (figure 3.8) and this had to be accounted for. Discussions on attenuation can be found in Koochesfahani and Dimotakis (1985), Daviero *et al.* (2001) and Tian and Roberts (2003).

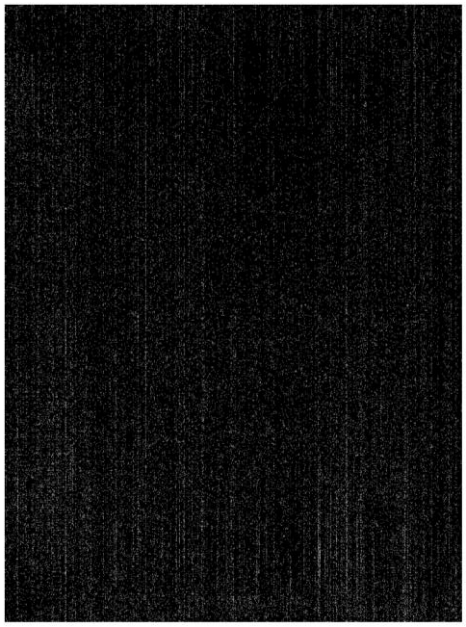

Figure 3.7: Image captured by covering the lens with contrast and brightness adjusted to make the noise visible.

Extensive post processing of the raw images was required to get the concentration data after accounting for all the above mentioned effects. The intensity value at each pixel for the image obtained by covering the lens was subtracted from the respective pixel value for all the raw images, which helped in correcting for the camera sensor noise.

$$I_c(i,k) = I_r(i,k) - I_b(i,k)$$

where $I_c(i,k)$, $I_r(i,k)$ and $I_b(i,k)$ are the (i,k)th pixel value for corrected, raw and lens covered image.

Now to account for the change in magnification, the scale factor was calculated considering middle plane as the reference.

$$Scale\ Factor = \frac{M_0}{M}$$

where M_0 was the magnification for middle plane while M was that for the plane being considered. The raw images were than resized using MATLAB function 'imresize'. The nearest-neighbor interpolation method was used where the output pixel is assigned the value that the point falls within (Adopted from MATLAB help). All resized images were then cropped to the size of image for the front plane. This ensured that all images had same geometric scale.

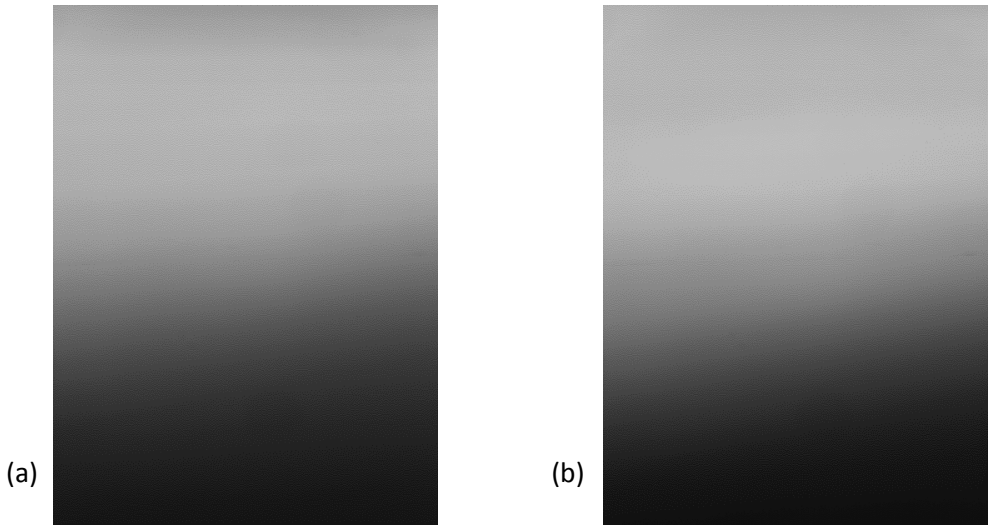

Figure 3.8: Reference image taken in the tank of water with known amount of Rhodamine 6G uniformly distributed using (a) laser head 1 and (b) laser head 2.

After the experiment was over, the tank was filled with some know amount of Rhodamine 6G. Reference images were taken for the laser sheet from each laser head separately (figure 3.8). The intensity value at each pixel for the previously corrected raw images at various planes was then divided by the same value for the reference image captured using respective laser head,

$$I_{cc}(i,k) = \frac{I_c(i,k)}{I_L(i,k)}$$

where$I_L(i,k)$ is the (i,k)th pixel value for reference image. This helped in accounting for the vignetting effects because of the lens and the laser sheet power attenuation effects.

3.6. Validation

As mentioned earlier, the 3D LIF system was applied on a steady axisymmetric round jet in quiescent ambient. The nozzle diameter was 2 mm and jet exit velocity was ~15 cm/s. The camera was made to record at 100 fps. The total scanned length was 140 mm with a frequency of 1 scan per second. The scanning rate was slow enough not to freeze the fluid at Kolmogorov scales, but fast for the larger scales to be considered frozen. The volume was scanned a total of 30 times as this was limited by the camera memory of 8 GB.

Few raw images that were captured by the camera at different planes are shown in figure 3.9. After correcting for errors, get 3D concentration field was reconstructed from two dimensional images. The reconstructed structure of the turbulent jet at an instant is shown in figure 3.10.

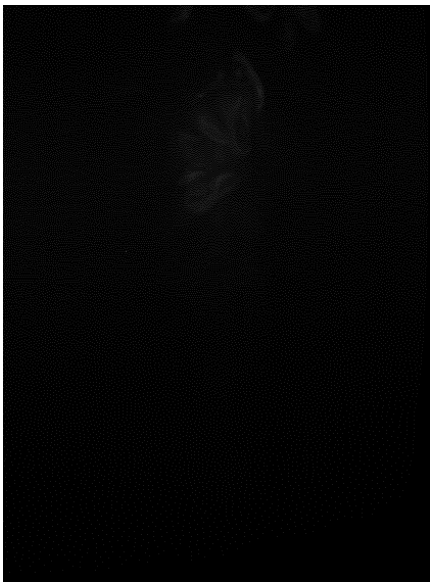

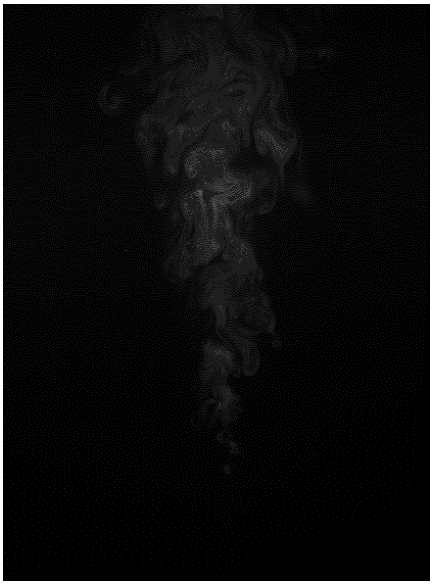

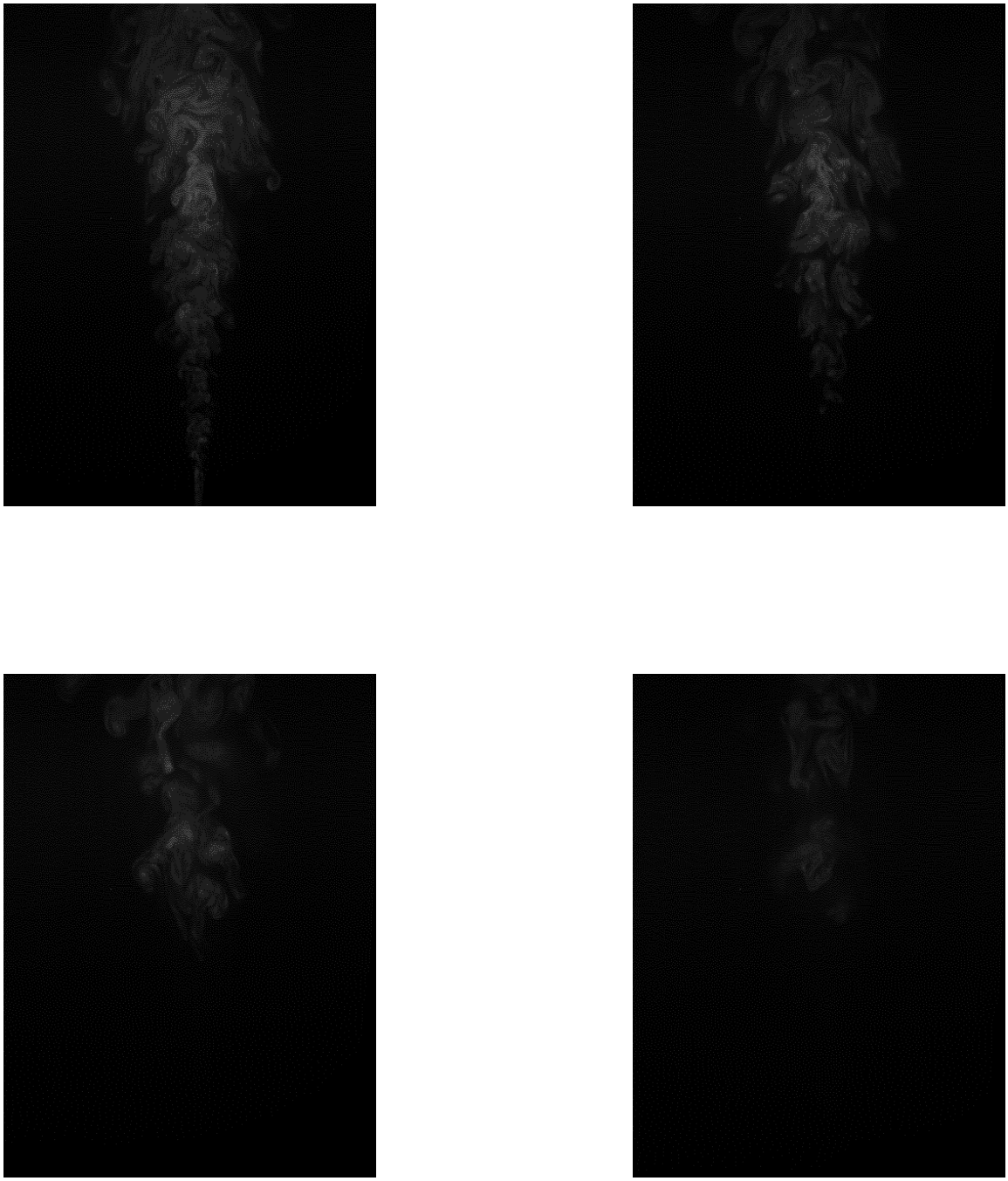

Figure 3.9: Raw images capured by camera at different planes with contrast and brightness adjusted.

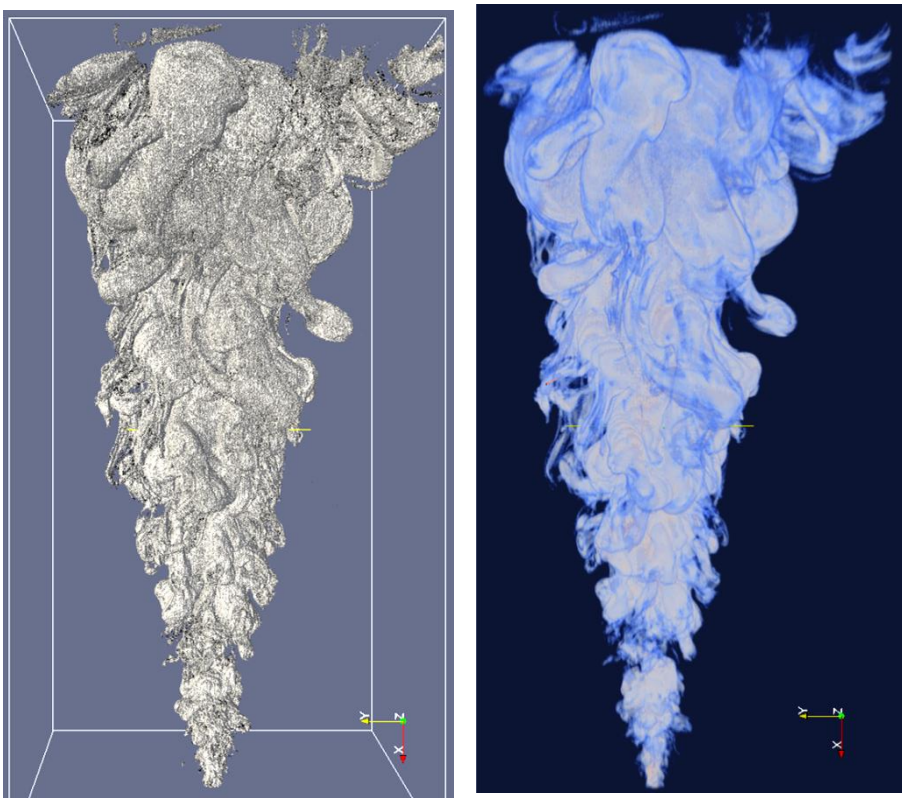

Figure 3.10: 3D structure of the jet at an instant.

Figure 3.11 (a) and 3.11 (b) shows vertical and horrizontal slices of concentration contours obtained from the time averaged three dimensional concentration field. The total concentration of scalar transported by jet is known to be always conserved (Cushman-Roisin, 2014). Figure3.12 show the mean change in concentration w.r.t time at all streamwise distances was always zero which showed the jet had achieved steady state. The structure of a time averaged turbulent jet is known to be a cone. Figure 3.13 shows change in cross sectonal area of a time averaged jet along the streamwise direction. It is quiet consistent with the quadratric fit with little departures. We believe that these departures were there because of limited data for time averaging.

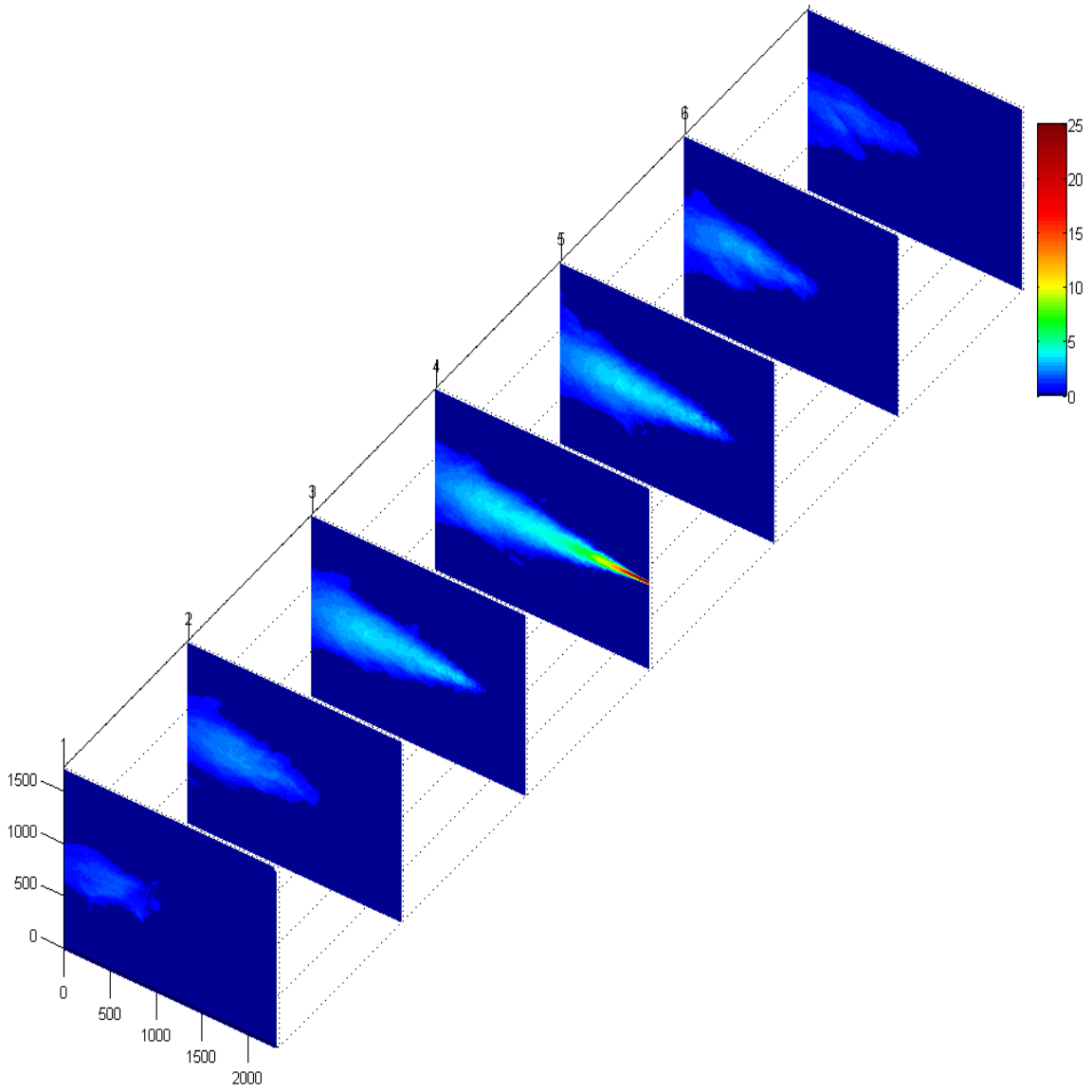

Figure 3.11 (a): Slices taken from the three dimensional structure showing concetration contours at various streamwise planes. Middle one is at the centre of the scanning volume and distance between the planes shown is 10 mm.

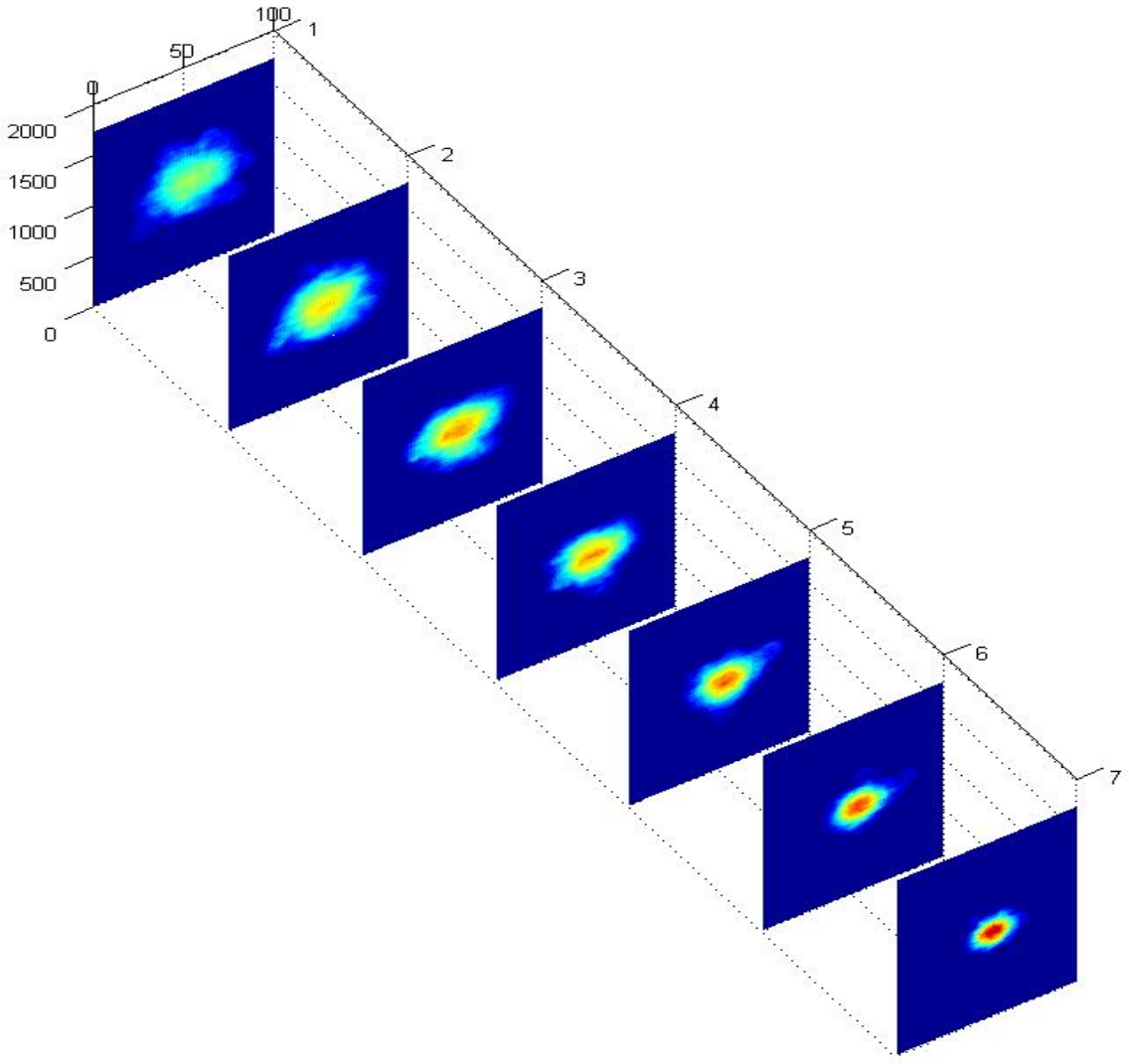

Figure 3.11 (b): Slices taken from the three dimensional concentration field showing concetration contours at lateral planes. Distance between slices is 20 mm.

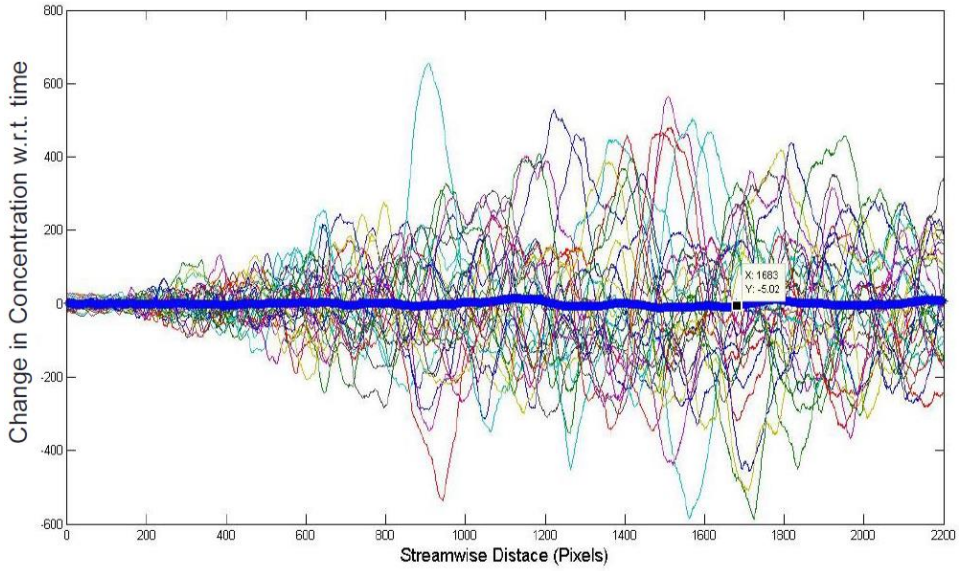

Figure 3.12: Plot showing change in total concentration w.r.t time at all streamwise locations. Blue line shows the mean value. (Geometric scale = 0.0992 mm/pixel)

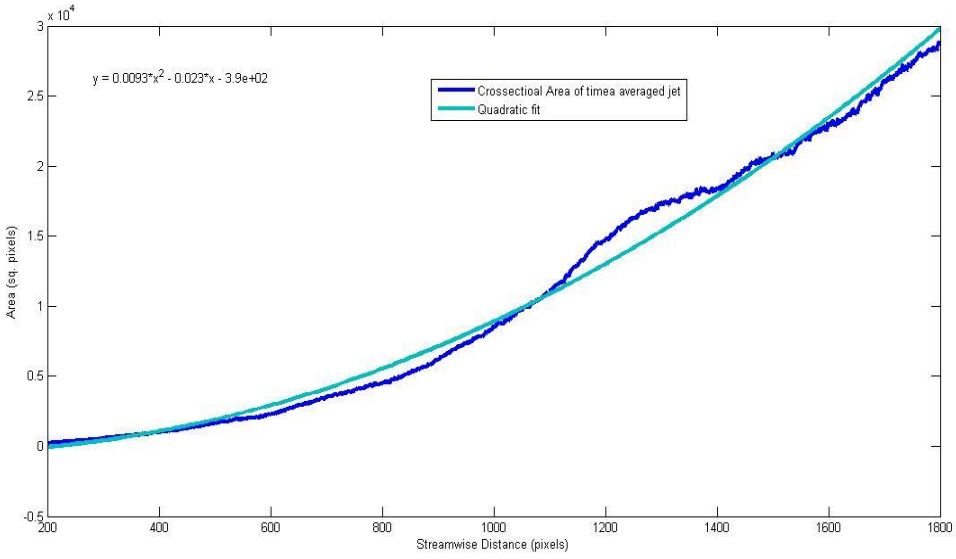

Figure 3.13: Plot showing change of cross sectonal area of a time averaged jet along the streamwise direction. (Geometric scale = 0.0992 mm/pixel)

The decay of maximum concenteration of a time averaged jet is shown in figure3.14. It agrees closely with the equation given by Fischer *et al.* (1979), i.e.

$$C_m = 5C_0\left(\frac{d}{x}\right).$$

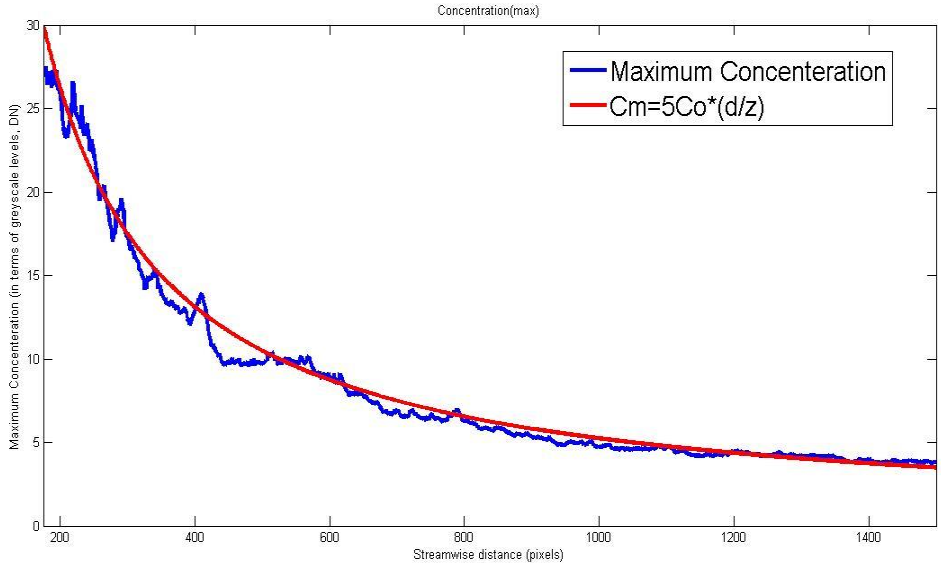

Figure 3.14: Plot showing variation of maximum concenteration along the streamwise direction in a time averaged jet. (Geometric scale = 0.0992 mm/pixel)

Figure 3.15 shows the mean concentration profiles for various stramwise directions. We believe that the profiles were not smooth because of limited data for time averaging. So we fitted the gaussian to the data by minimising the absolute error using fminsearch MATLAB function. The Gaussian fitted profiles in the direction parallel and normal to the plane of the laser are shown in figure 3.16. The profiles in the plane normal to the plane of the laser sheet also showed a nice collapese at various streamwise distances. This proved the consistancy of our setup. The jet half width found from the gaussian fitted profiles was found to be varying as 0.130*z (figure 3.17) which was consistent with range given by Fischer

et al. (1979). The jet was found to be little tilted in plane of laser sheet (Figure 3.18). This variation could be because of the jet being tilted or the reynolds number being low, the jet was not able to attain complete self similarity. But oveall, this technique was able to capture the three dimensional scalar structure of the turbulent jet.

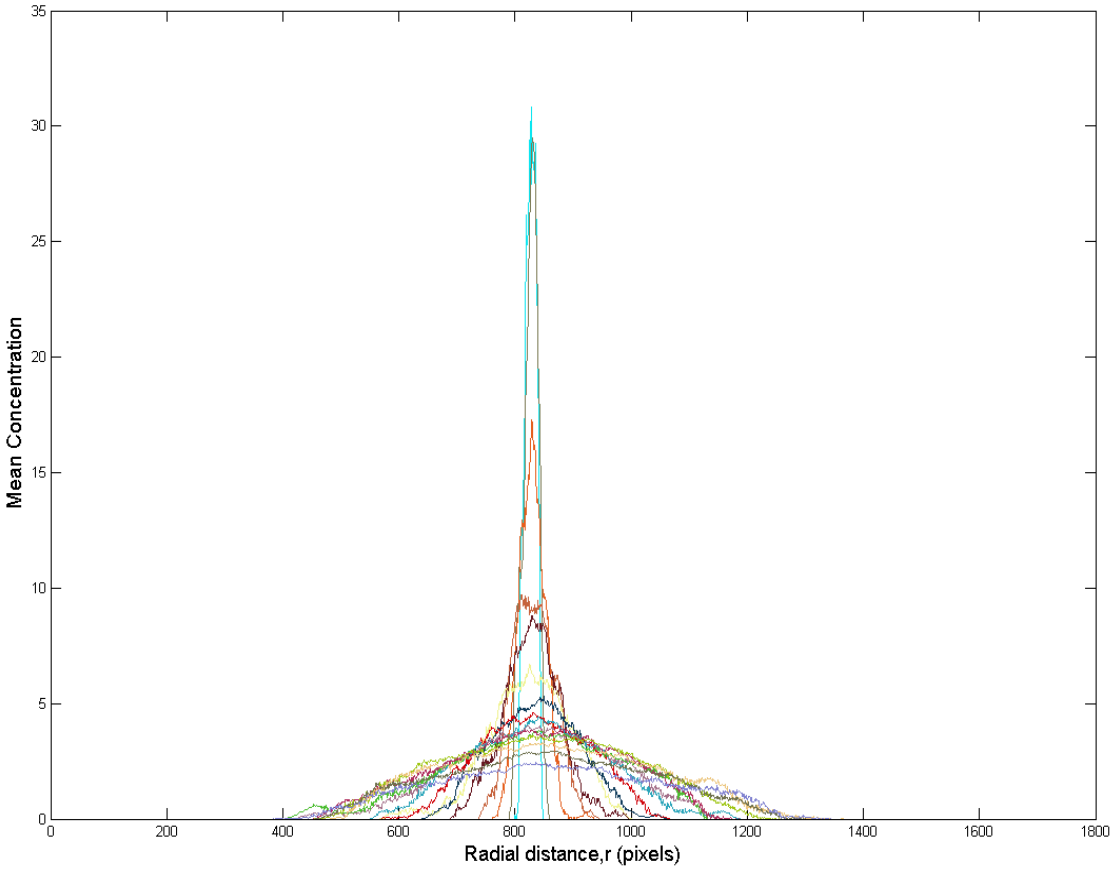

Figure 3.15: Plot showing mean axial concentraion profiles at various streamwise locations.(Geometric scale = 0.0992 mm/pixel)

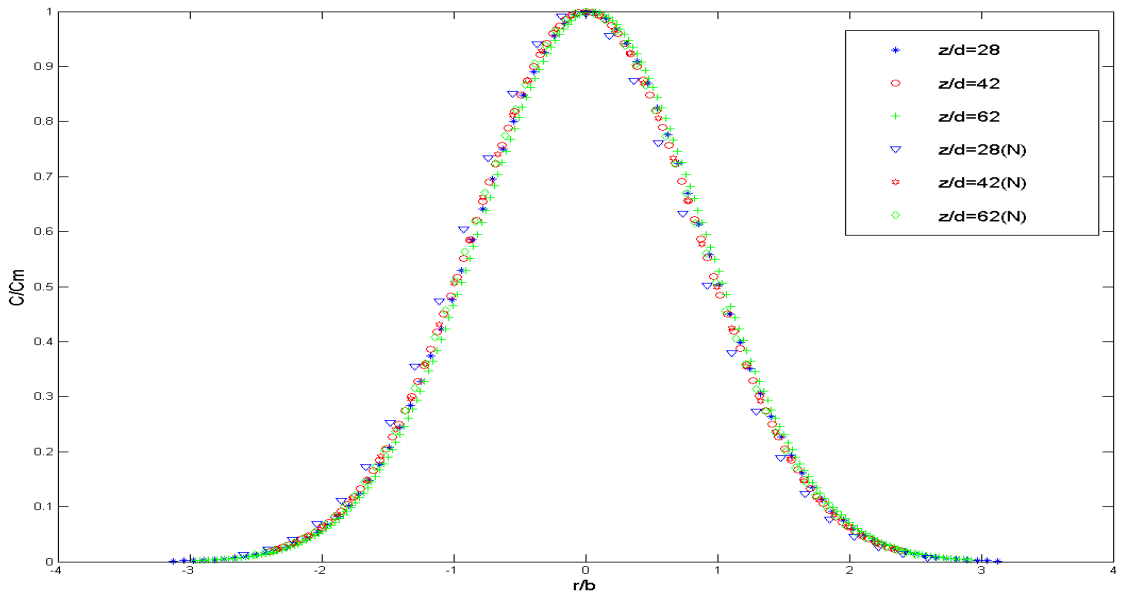

Figure 3.16: Plot showing fitted Gaussian axial concentration profiles. (N) corresponds to plane normal to the plane of laser sheet and in line with nozzle centre.

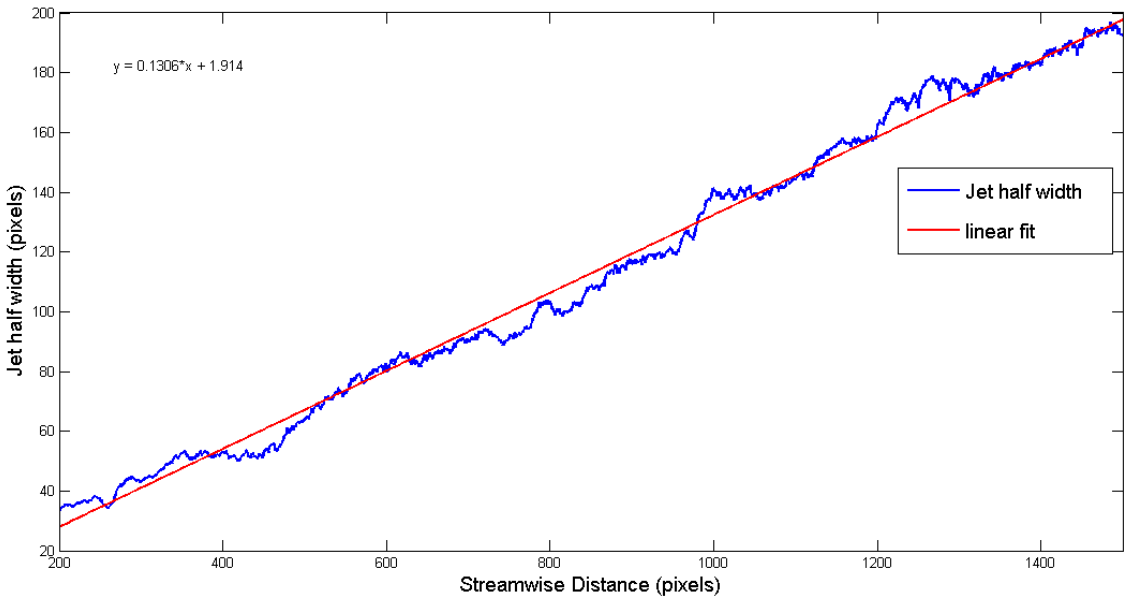

Figure 3.17: Plot showing varation of jet half width in the streamwise direction.(Geometric scale = 0.0992 mm/pixel)

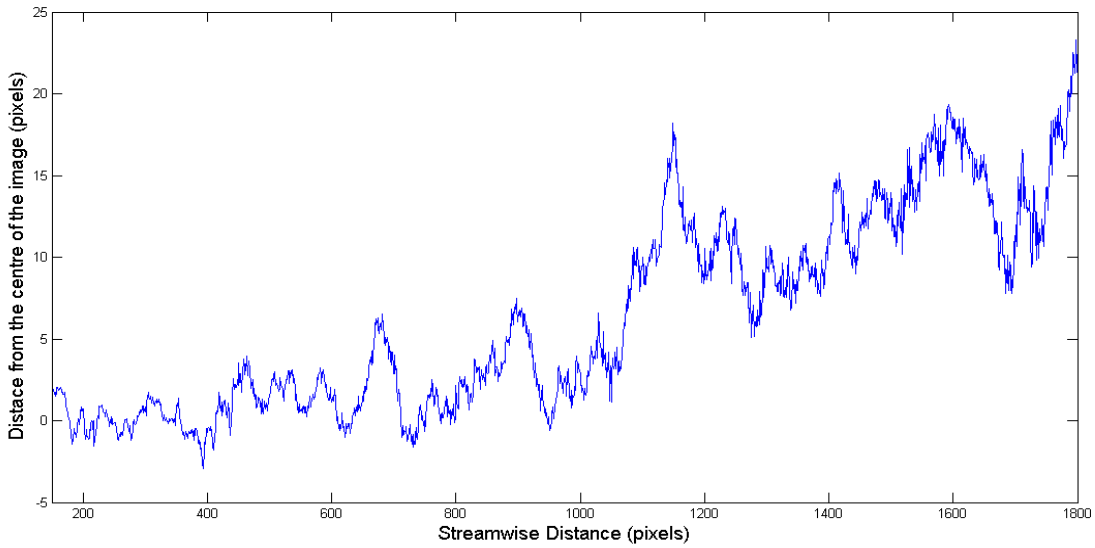

Figure 3.18: Variation of the peak in Gaussian fitted profiles in the streamwise direction. (Geometric scale = 0.0992 mm/pixel)

3.7. Preliminary Results

Now after validating the robostness of the reported technique, we used the mean concentration values at the middle plane to find the scalar edge of the jet (figure 3.19). We plotted the fitted mean concentration profiles at various z/d sections. Then we checked for points where concentration reduces to a small fraction of the maximum value on either side. We tried this for various fractional values and fitted a linear plot through those points. We found that plot fitted to points where concentration reduces to 10% of the maximum value most closely resembled to the edge of the jet.

We considered the line representing 10% of maximum concentration as the edge of the time averaged steady jet. Now using the three dimensional structure of the jet, we found how the coloured area (dyed fluid area) at a streamwise location in the cross section at an instant changes with respect to that in a steady mean jet

(figure 3.20). Basically we calculated ratio of coloured fluid area to the area calculated using the edge of the mean jet.

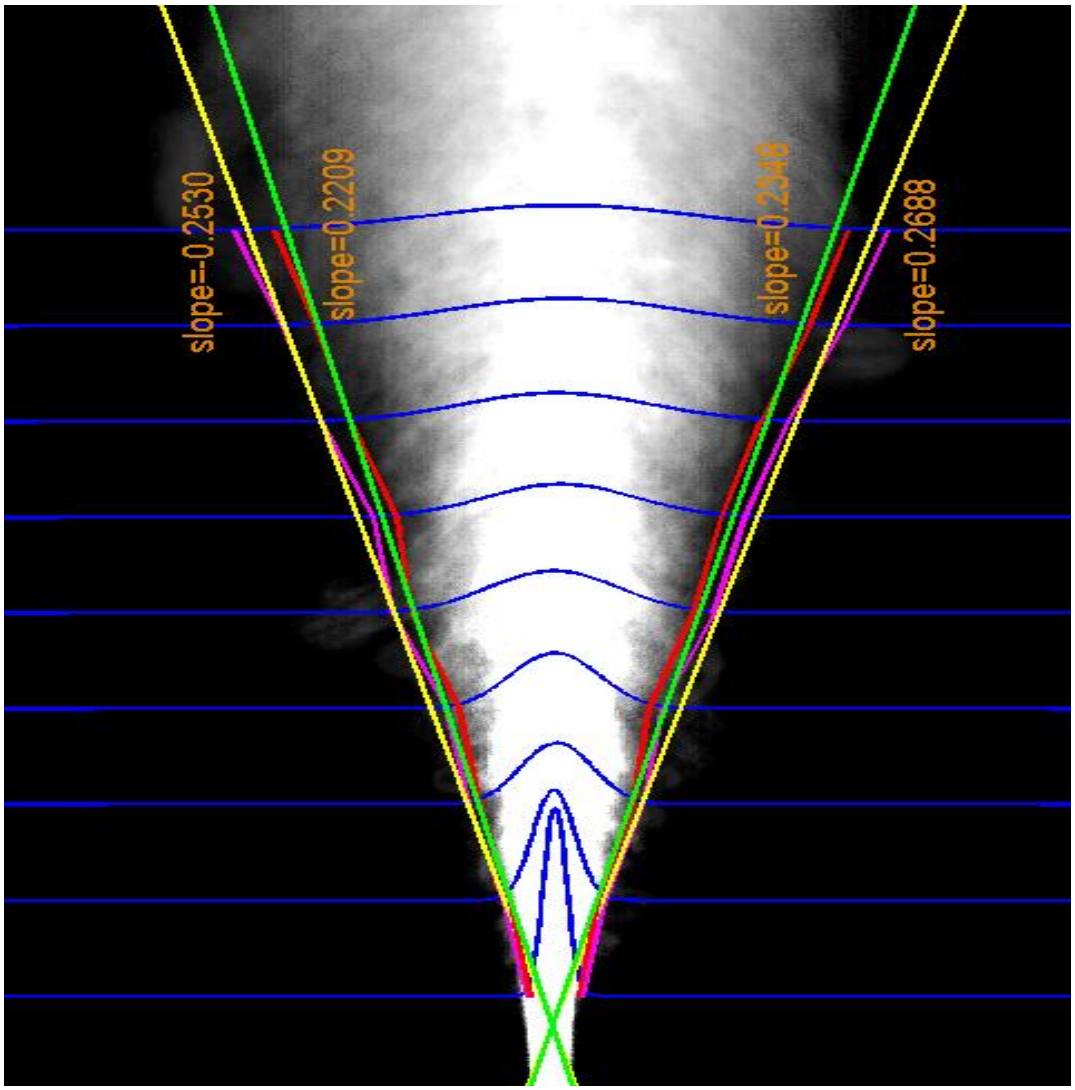

Figure 3.19: This pictue shows the time averaged jet vertical cross section. Blue lines represent the concentration profile at that streamwise location. Bottommost profile is at z/d=5 and the distance between two profile location is z/d=7.5. Pink and Red lines are the lines connecting points where concentration is 5% and 10% of maximum concentration respectively at various shown z/d locations. Yellow and Green lines are the linear fitted lines of the 5% and 10% of the maximum concentration data respectively.

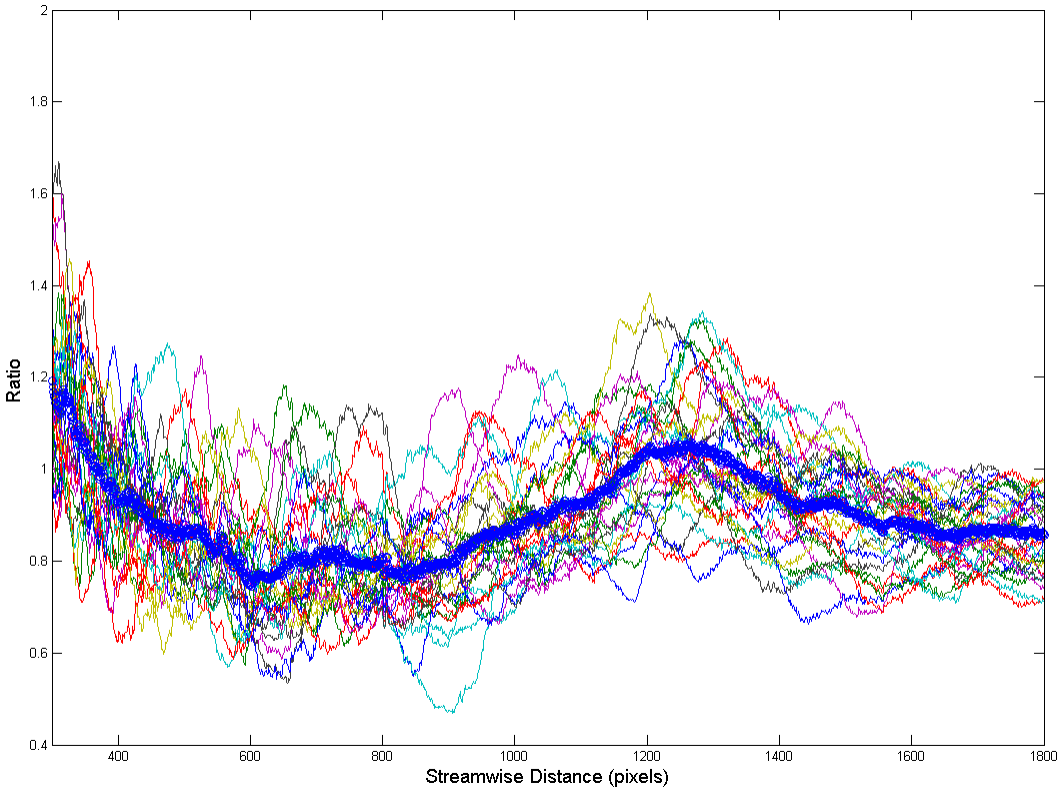

Figure 3.20: Plot showing variation of ratio of area at a cross section between dyed region and to that of mean steady jet along the streamwise direction. Thin coloured lines show the variation of the ratio for 31 separate instances while thick blue line shows the mean of the ratio variation for 31 instances.

The idea behind doing this was to get some information regarding quantity of ambient fluid entering the main jet flow which basically would be a colourless fluid in the region of dyed fluid. This kind of information can be very helpful in understanding cloud flows as the air entrained in the cloud would be free of water droplets. We plotted the mean for the ratio of area of coloured fluid to that for a mean jet structure (figure 3.20). It was found that the mean ratio here was very different from the expected constant ratio (=1) line. It was seen that the mean ratio plot reduces to minimum of approximately 0.8 at z/d of 25 (600 pixels streamwise

distance), rises again to expected constant ratio line by z/d of 55 and then starts to decrease again. This could be because of limited data for averaging. But the most strange thing observed was that the mean ratio never rose above unity between z/d of 5 to z/d of 85.

But to say anything conclusively, many more sets of experiments are required.

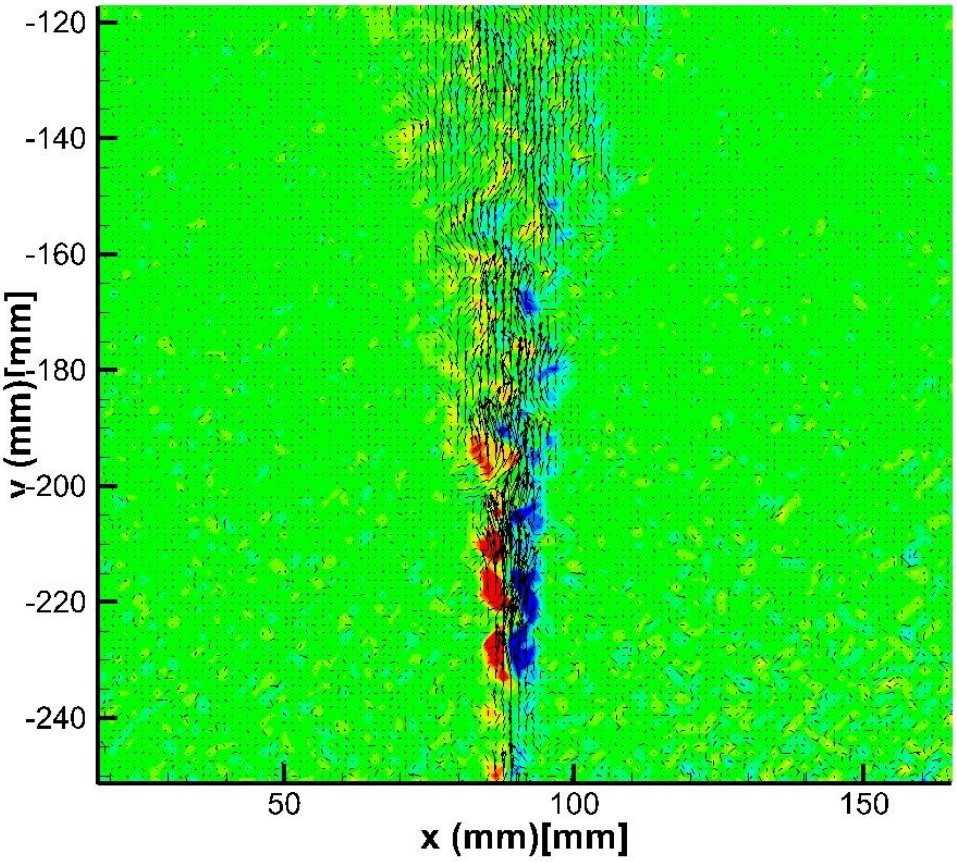

Figure 3.21: Instantaneous vorticity contours overlapped with velocity vectors for a steady jet. (Obtained using Dantec Dynamic Studio)

We were also able to obtain the the vorticiy and velocity at the centre section using PIV. Instantanous image of vorticity contours overlapped with velocity vectors is shown in figure 3.21. Now using PIV and scanning setup, 3D velocity field could also be obtained using same setup.

CHAPTER 4

CONCLUSIONS AND SCOPE FOR FUTURE WORK

The thesis contains two parts: in the first part we present, a laboratory model to simulate orographic clouds and in the second part we report an improved optical tomography technique.

Orographic clouds are formed when moist air is forced to rise along the mountain slope. The latent heat released as a result of phase change will have a significant effect on the structure of the flow. In this thesis, planar turbulent wall jet with volumetric heat addition was considered as a low order model for simulating cloud flows. The apparatus was designed and fabricated which is capable of producing a vertical wall jet with volumetric heat addition. The apparatus, fixed on a screw jack mechanism which could be made inclined at a desired angle to the vertical to mimic the mountain slope. Initial flow visualization showed that apparatus was capable of producing a continuous turbulent wall jet at various angles. A set of heating grids were designed and fixed parallel to the wall in order to volumetrically heat the flow, mimicking the latent heat released due to condensation in real clouds. Planar laser induced fluorescence (PLIF) images showed that the scalar width of wall jet decreases drastically with the addition of heat which is consistent with real orographic clouds as they rise as a layer, hugging along the mountain slope.

An improved optical topographic technique presented here, is based on sweeping a laser sheet across the turbulent shear flow, while ensuring that the sheet is always parallel and visualize the flow using laser induced fluorescence to obtain a tomography image. The materials used for the development were conveniently available and were relatively inexpensive than previously reported

techniques. This technique could be used to study the time evolution of scalar field in turbulent shear flows. This new method is robust enough, as was verified by applying the same for an axisymmetric round jet and the data was well in agreement with that reported in the literature.

This newly devised technique combined with presented laboratory model for orographic clouds could be used in future to study the time evolution of the scalar concentration field. This can help in understanding the water vapour/droplet distribution in a real cloud and in turn, help to discern the reason behind "entrainment anomalies" observed in clouds. This kind of study could also give an insight to dynamics of wall flames, which have very similar mechanism and are of huge importance in the field of combustion.

New method of tomographic LIF reported in this thesis could also be further extended to get the three dimensional velocity fields in a turbulent shear flow using particle image velocimetry (PIV). This requires camera to take two frames at same section, thereby requiring the laser sheet to move intermittently, ensuring that the two successive laser pulses illuminate the flow at the same vertical section. This could be achieved either by making a screw rod rotate intermittently using some intermittent rotary mechanism or by using an octagonal prism rotating continuously at some appropriate speed which will make the laser sheet to move back to the previous position in the time between the two camera frames.

REFERENCES

Agrawal, A., & Prasad, A. K. (2004). Evolution of a turbulent jet subjected to volumetric heating. *Journal of Fluid Mechanics*, *511*, 95-123.

Arakawa, A. (2004). The cumulus parameterization problem: Past, present, and future. *Journal of Climate*, *17*(13), 2493-2525.

Baines, P. G. (1987). Upstream blocking and airflow over mountains. *Annual review of fluid mechanics*, *19*(1), 75-95.

Barenblatt, G. I., Chorin, A. J., & Prostokishin, V. M. (2005). The turbulent wall jet: A triple-layered structure and incomplete similarity. *Proceedings of the National Academy of Sciences of the United States of America*, *102*(25), 8850-8853.

Basu, A. J., & Narasimha, R. (1999). Direct numerical simulation of turbulent flows with cloud-like off-source heating. *Journal of Fluid Mechanics*, *385*, 199-228.

Belcher, S. E., & Hunt, J. C. R. (1998). Turbulent flow over hills and waves. *Annual Review of Fluid Mechanics*, *30*(1), 507-538.

Bhat, G. S., Narasimha, R., & Arakeri, V. H. (1989). A new method of producing local enhancement of buoyancy in liquid flows. *Experiments in fluids*, *7*(2), 99-102.

Bhat, G. S., & Narasimha, R. (1996). A volumetrically heated jet: large-eddy structure and entrainment characteristics. *Journal of Fluid Mechanics*, *325*, 303-330.

Blyth, A. M. (1993). Entrainment in cumulus clouds. *Journal of applied meteorology*, *32*(4), 626-641.

Boos, W. R., & Kuang, Z. (2010). Dominant control of the South Asian monsoon by orographic insulation versus plateau heating. *Nature*, *463*(7278), 218-222.

Chakraborty, A., Nanjundiah, R. S., & Srinivasan, J. (2002). Role of Asian and African orography in Indian summer monsoon. *Geophysical research letters*,*29*(20), 50-1.

Chandrasekar, A. (2010). *Basics of Atmospheric Science*. PHI Learning Pvt. Ltd..

Charney, J. G. & Shukla., J., *Predictability of monsoons, in Monsoon Dynamics*, M.J. Lighthill and R.P. Pierce, eds., Cambridge University Press, Cambridge, 1981, pp. 99–109.
Corby, G. A. (1954). The airflow over mountains. A review of the state of current knowledge. *Quarterly Journal of the Royal Meteorological Society*, *80*(346), 491-521.

Dahm, W. J., Southerland, K. B., & Buch, K. A. (1991). Direct, high resolution, four-dimensional measurements of the fine scale structure of Sc≫ 1 molecular mixing in turbulent flows. *Physics of Fluids A: Fluid Dynamics (1989-1993)*, *3*(5), 1115-1127.

Dash, S. K., & Mohandas, S. (2005). Comparative study of different orographic representations with respect to the Indian summer monsoon simulation. *Acta Geophysica Polonica*, *53*(3), 325.

Dejoan, A., & Leschziner, M. A. (2005). Large eddy simulation of a plane turbulent wall jet. *Physics of Fluids (1994-present)*, *17*(2), 025102.

Delo, C., & Smits, A. J. (1997). Volumetric visualization of coherent structure in a low Reynolds number turbulent boundary layer. *International Journal of Fluid Dynamics*, *1*, 3.

Dimotakis, P. E., Miake-Lye, R. C., & Papantoniou, D. A. (1983). Structure and dynamics of round turbulent jets. *Physics of Fluids*, *26*(11), 3185-3192.

Diwan, S. S., Narasimha, R., Bhat, G. S., & Sreenivas, K. R. (2011, December). Laboratory studies of anomalous entrainment in cumulus cloud flows. In *Journal of Physics: Conference Series* (Vol. 318, No. 7, p. 072014). IOP Publishing.

Emanuel, K. A. (1994). *Atmospheric convection*. Oxford University Press.

Eriksson, J. G., Karlsson, R. I., & Persson, J. (1998). An experimental study of a two-dimensional plane turbulent wall jet. *Experiments in fluids*, *25*(1), 50-60.

Fischer, H. B. (Ed.). (1979). *Mixing in inland and coastal waters*. Academic press.

George, W. K., Abrahamsson, H., Eriksson, J., Karlsson, R. I., Löfdahl, L., & Wosnik, M. (2000). A similarity theory for the turbulent plane wall jet without external stream. *Journal of Fluid Mechanics*, *425*, 367-411.

Glauert, M. B. (1956). The wall jet. *Journal of Fluid Mechanics*, *1*(06), 625-643.

Guezennec, Y. G., Yang, Z., & Gieseke, T. J. (1996). High-speed 3-D scanning particle image velocimetry (3-D SPIV) technique. In *Developments in Laser Techniques and Applications to Fluid Mechanics* (pp. 392-407). Springer Berlin Heidelberg.

Hahn, D. G., & Manabe, S. (1975). The role of mountains in the south Asian monsoon circulation. *Journal of the Atmospheric Sciences*, *32*(8), 1515-1541.

Heus, T., & Jonker, H. J. (2008). Subsiding shells around shallow cumulus clouds. *Journal of the Atmospheric Sciences*, *65*(3), 1003-1018.

Houze Jr, R. A. (1994). *Cloud dynamics* (Vol. 53). Academic press.

Karlsson, R. I., Eriksson, J., & Persson, J. (1992). *LDV measurements in a plane wall jet in a large enclosure*. ROYAL INST OF TECH STOCKHOLM (SWEDEN).

Koochesfahani, M., & Dimotakis, P. E. (1985). Laser-induced fluorescence measurements of mixed fluid concentrationin a liquid plane shear layer. *AIAA journal*, *23*(11), 1700-1707.

Launder, B. E., & Rodi, W. (1981). The turbulent wall jet. Prog. *Aerospace Science*, *19*, 81-128.

Launder, B. E., & Rodi, W. (1983). The turbulent wall jet measurements and modeling. *Annual Review of Fluid Mechanics*, *15*(1), 429-459.

List, E. J. (1982). Turbulent jets and plumes. *Annual Review of Fluid Mechanics*,*14*(1), 189-212.

Lockwood, M., & Fröhlich, C. (2008). Recent oppositely directed trends in solar climate forcings and the global mean surface air temperature. II. Different reconstructions of the total solar irradiance variation and dependence on response time scale. *Proceedings of the Royal Society A: Mathematical, Physical and Engineering Science*, *464*(2094), 1367-1385.

Ludlam, F. H., & Scorer, R. S. (1957). Cloud study. A pictorial guide. *Cloud study. A pictorial guide*.

Ma, D., Boos, W., & Kuang, Z. (2014). Effects of Orography and Surface Heat Fluxes on the South Asian Summer Monsoon. *Journal of Climate*, (2014).

Manikandan, M. S. (2005). Effects of viscosity on the entrainment and dynamics of a buoyant jet, PhD Thesis.

Mehta, R. D., & Bradshaw, P. (1979). Design rules for small low-speed wind tunnels. *Aeronautical Journal*, *83*(827), 443-449.

Merkel, G. J., Rys, P., Rys, F. S., & Dracos, T. A. (1996). Concentration and velocity field measurements in turbulent flows using laser-induced fluorescence tomography (LIFT). *Applied Scientific Research*, *56*(2-3), 181-190.

Morton, B. R., Taylor, G., & Turner, J. S. (1956). Turbulent gravitational convection from maintained and instantaneous sources. *Proceedings of the Royal Society of London. Series A. Mathematical and Physical Sciences*,*234*(1196), 1-23.

Narasimha, R., & Bhat, G. S. (2008, January). Recent experimental and computational studies related to the fluid dynamics of clouds. In *IUTAM Symposium on Computational Physics and New Perspectives in Turbulence* (pp. 313-320). Springer Netherlands.

Narasimha, R., Diwan, S. S., Duvvuri, S., Sreenivas, K. R., & Bhat, G. S. (2011). Laboratory simulations show diabatic heating drives cumulus-cloud evolution and entrainment. *Proceedings of the National Academy of Sciences*, *108*(39), 16164-16169.

Narasimha, R. (2012). Cumulus clouds and convective boundary layers: a tropical perspective on two turbulent shear flows. *Journal of Turbulence*, (13).

Paluch, I. R. (1979). The entrainment mechanism in Colorado cumuli. *Journal of the atmospheric sciences*, *36*(12), 2467-2478.

Patrie, B. J., Seitzman, J. M., & Hanson, R. K. (1994). Instantaneous three-dimensional flow visualization by rapid acquisition of multiple planar flow images.*Optical Engineering*, *33*(3), 975-980.

Prasad, R. R., & Sreenivasan, K. R. (1990). Quantitative three-dimensional imaging and the structure of passive scalar fields in fully turbulent flows. *Journal of Fluid Mechanics*, *216*, 1-34.

Prasanth, P. (2014). Direct numerical simulation of transient cumulus cloud flow. MS(Engg.) Thesis.

Rajaratnam, N. (1976). *Turbulent jets*. Elsevier.

Ramaswamy, V., Boucher, O., Haigh, J., Hauglustaine, D., Haywood, J., Myhre, G., Nakajima, T., Shi, G. & Solomon, S. 2001 Climate change 2001: The scientific basis: *Contribution of working group I to the Third Assessment Report of the Intergovernmental Panel on Climate Change* 8510.

Reuter, G. W. (1986). A historical review of cumulus entrainment studies.*Bulletin of the American Meteorological Society*, *67*(2), 151-154.

Riehl, H., & Malkus, J. S. (1958). On the heat balance in the equatorial trough zone. *Geophysica*, *6*(3-4), 503-538.

Roberts, P. J., Maile, K., & Daviero, G. (2001). Mixing in stratified jets. *Journal of Hydraulic Engineering*, *127*(3), 194-200.

Romps, D. M., & Kuang, Z. (2010). Do undiluted convective plumes exist in the upper tropical troposphere?. *Journal of the Atmospheric Sciences*, *67*(2), 468-484.

Ruck, B., & Pavlovski, B. (2000). Laser tomography for flow structure analysis. *High Temperature*, *38*(1), 106-117.

Sawyer, J. S. (1956). The physical and dynamical problems of orographic rain.*Weather*, *11*(12), 375-381.

Schneider, M. E., & Goldstein, R. J. (1994). Laser Doppler measurement of turbulence parameters in a two-dimensional plane wall jet. *Physics of Fluids (1994-present)*, *6*(9), 3116-3129.

Shan, J. W., Lang, D. B., & Dimotakis, P. E. (2004). Scalar concentration measurements in liquid-phase flows with pulsed lasers. *Experiments in fluids*,*36*(2), 268-273.

Simpson, J. (1983). Cumulus clouds: Early aircraft observations and entrainment hypotheses. In *Mesoscale Meteorology—Theories, Observations and Models*(pp. 355-373). Springer Netherlands.

Sloss, P. W. (1967). An empirical examination of cumulus entrainment. *Journal of Applied Meteorology*, *6*(5), 878-881.

Squires, P. (1958). Penetrative downdraughts in cumuli. *Tellus*, *10*(3), 381-389.

Squires, P., & Turner, J. S. (1962). An entraining jet model for cumulo-nimbus updraughts. *Tellus*, *14*(4), 422-434.

Starr Malkus, J. (1954). Some results of a trade-cumulus cloud investigation.*Journal of Meteorology*, *11*(3), 220-237.

Stommel, H. (1947). ENTRAINMENT OF AIR INTO A CUMULUS CLOUD: (Paper presented 27 December 1946 at the Annual Meeting, AMS, Cambridge, Massachusetts). *Journal of Meteorology*, *4*(3), 91-94.

Sreenivas, K. R. (2004, 17-21 May). Study of entrainment process in a planar jet using diffusion-vortex method, *Proceedings of The Tenth Asian Congress of Fluid Mechanics, B33, Peradeniya, Sri Lanka.*

Sreenivas, K. R., & Prasad, A. K. (2000). Vortex-dynamics model for entrainment in jets and plumes. *Physics of Fluids (1994-present)*, *12*(8), 2101-2107.

Svensmark, H., & Friis-Christensen, E. (1997). Variation of cosmic ray flux and global cloud coverage—a missing link in solar-climate relationships. *Journal of Atmospheric and Solar-Terrestrial Physics*, *59*(11), 1225-1232.

Stratmann, F., Moehler, O., Shaw, R., & Heike, W. (2009). Laboratory cloud simulation: Capabilities and future directions. *Clouds in the Perturbed Climate System: Their Relationship to Energy Balance, Atmospheric Dynamics, and Precipitation*, 149-172.

Tachie, M. F. (2001). Open channel turbulent boundary layers and wall jets on rough surfaces, PhD Thesis.

Taylor, G. I. (1946). *Dynamics of a mass of hot gas rising in air*. Technical Information Division, Oak Ridge Operations.

Telford, J. W. (1975). Turbulence, entrainment, and mixing in cloud dynamics.*pure and applied geophysics*, *113*(1), 1067-1084.

Tian, X., & Roberts, P. J. (2003). A 3D LIF system for turbulent buoyant jet flows.*Experiments in Fluids*, *35*(6), 636-647.

Turner, J. S. (1963). Model experiments relating to thermals with increasing buoyancy. *Quarterly Journal of the Royal Meteorological Society*, *89*(379), 62-74.

Turner, J. S. (1969). Buoyant plumes and thermals. *Annual Review of Fluid Mechanics*, *1*(1), 29-44.

Turner, J. (1983). S. 1973 Buoyancy effects in Fluids.

Turner, J. S. (1986). Turbulent entrainment: the development of the entrainment assumption, and its application to geophysical flows. *Journal of Fluid Mechanics*,*173*, 431-471.

Van Cruyningen, I., Lozano, A., & Hanson, R. K. (1990). Quantitative imaging of concentration by planar laser-induced fluorescence. *Experiments in Fluids*,*10*(1), 41-49.

Venkatakrishnan, L., Bhat, G. S., Prabhu, A., & Narasimha, R. (1998). Visualization studies of cloud-like flows. *Current Science*, *74*(7), 597-606.

Venkatakrishnan, L., Bhat, G. S., & Narasimha, R. (1999). Experiments on a plume with off-source heating: Implications for cloud fluid dynamics. *Journal of Geophysical Research: Atmospheres (1984–2012)*, *104*(D12), 14271-14281.

Venkatakrishnan, L., Elavarasan, R., Bhat, G. S., Krothapalli, A., & Lourenco, L. (2003). Particle image velocimetry study of a cloud-like flow. *Current Science*,*85*(6), 778-785.

Wang, Y., Leung, L. R., McGREGOR, J. L., Lee, D. K., Wang, W. C., Ding, Y., & Kimura, F. (2004). Regional climate modeling: progress, challenges, and prospects. *気象集誌. 第 2 輯*, *82*(6), 1599-1628.

Warner, J. (1955). The water content of cumuliform cloud. *Tellus*, *7*(4), 449-457.